Materials Today Bio 32 (2025) 101896

Contents lists available at ScienceDirect

Materials Today Bio

journal homepage: www.journals.elsevier.com/materials-today-bio

Quercetin-loaded exosomes delivery system prevents myopia progression by targeting endoplasmic reticulum stress and ferroptosis in scleral fibroblasts

Lianghui Zhao [a,b], Xiaoyun Dong [a,b], Bin Guo [a,*], Jike Song [a,**], Hongsheng Bi [b,c,***]

[a] Shandong University of Traditional Chinese Medicine, Jinan, 250014, China
[b] Affiliated Eye Hospital of Shandong University of Traditional Chinese Medicine, Jinan, 250002, China
[c] Shandong Provincial Key Laboratory of Integrated Traditional Chinese and Western Medicine for Prevention and Therapy of Ocular Diseases, Shandong Academy of Eye Disease Prevention and Therapy, Jinan, 250002, China

ARTICLE INFO

Keywords:
Quercetin
Myopia
Ferroptosis
Endoplasmic reticulum stress
Drug delivery

ABSTRACT

Myopia, a predominant cause of visual impairment, is often associated with scleral extracellular matrix (ECM) remodeling and axial elongation. Currently, effective therapeutic strategies for addressing scleral ECM remodeling remain limited, necessitating the development of new treatments. Quercetin, a natural flavonoid, has been shown to alleviate ECM remodeling. However, its hydrophobic nature limits clinical application. To address this, we developed a quercetin-loaded exosome delivery system (Exo-Que) to enhance quercetin bioavailability and investigated its effects and mechanisms in myopia prevention. This system exhibited excellent aqueous solubility, enhanced corneal permeability, and prolonged precorneal retention, enabling low-dose administration with significant efficacy. In the initial phase of treatment, Exo-Que showed a pronounced myopia prevention effect, with reductions of 58.41 % in refractive error progression and 38.46 % in axial length growth after two weeks of treatment. As the treatment duration extended to four weeks, its therapeutic efficacy remained robust, achieving reductions of 59.97 % and 35.85 %, respectively. The therapeutic efficacy of Exo-Que was comparable to that of the 0.1 % atropine group (at two weeks, reducing 59.07 % and 35.9 %, respectively; at four weeks, 59.84 % and 37.74 %, respectively). Mechanistically, Exo-Que inhibited the activation of the IRE1-XBP1, PERK-eIF2, and ATF6 pathways, alleviating endoplasmic reticulum stress. Furthermore, it suppressed ferroptosis by modulating GRP78-ACSL4 and GRP78-GPX4 protein interactions, thus mitigating ECM remodeling and slowing myopia progression. Besides, Exo-Que showed excellent biosafety in both *in vitro* and *in vivo* studies. Collectively, these results highlight the promising therapeutic potential of Exo-Que for myopia prevention.

1. Introduction

Myopia is an extremely widespread ocular disorder, which has emerged as an urgent global concern due to its rapidly escalating prevalence [1,2]. Similar to other complex diseases, the underlying mechanism of myopia remains incompletely understood. Numerous studies have verified that myopia is often accompanied by scleral extracellular matrix (ECM) remodeling, which can reduce scleral strength and thickness, weaken its mechanical support in maintaining the shape of the eyeball, and subsequently result in axial length (AL) elongation [3,4]. Although scleral hypoxia, inflammation, and mechanical stress had been implicated in scleral ECM remodeling during myopia development [5–8], the precise mechanisms were not yet fully elucidated. Therefore, it is still imperative and challenging to explore the mechanism and develop novel control strategies with high efficacy for myopia control.

Scleral fibroblasts, the most preponderant cells in scleral ECM, are responsible for synthesizing all ECM components and play a crucial role in scleral ECM remodeling during myopia progression [3,4]. Recently, new evidence confirms that endoplasmic reticulum (ER) stress in scleral fibroblasts mediates scleral ECM remodeling [9,10]. ER stress is a protective cellular response aimed at maintaining homeostasis. When ER

* Corresponding author.
** Corresponding author.
*** Corresponding author. Affiliated Eye Hospital of Shandong University of Traditional Chinese Medicine, Jinan, 250002, China.
E-mail addresses: guobin00002@126.com (B. Guo), edusjk@163.com (J. Song), bihongsheng@sdutcm.edu.cn (H. Bi).

https://doi.org/10.1016/j.mtbio.2025.101896
Received 11 January 2025; Received in revised form 12 May 2025; Accepted 22 May 2025
Available online 28 May 2025

homeostasis is disrupted, cells upregulate GRP78 to assist with protein refolding and activate key signaling pathways, including IRE1, PERK, and ATF6, to initiate the unfolded protein response (UPR). This response contributes to increase in protein-folding capacity and restores homeostasis [11,12]. However, prolonged UPR activation can induce a complex signaling pathways network leading to cell death, such as apoptosis, autophagy, ferroptosis, and so on [13]. Ferroptosis, as a new form of cell death dependent on lipid peroxidation and iron overload, had been proven to promote ECM remodeling in other fibrotic diseases [14,15]. Owing to the fact that ECM remodeling drives myopia progression and effective therapeutic strategies for it remain scarce, the development of promising and targeted strategies for myopia control is highly urgent. Kazuo Tsubota et al. reported that 4-phenylbutyric acid could alleviate ER stress-mediated scleral ECM remodeling, and then significantly inhibit AL prolongation in mice [9]. These findings suggest that targeting ER stress and ferroptosis in scleral fibroblasts might be an appealing strategy to inhibit scleral ECM remodeling and retard myopia progression.

Quercetin, as a flavonoid possesses rich biological activity and high medicinal value, is naturally distributed in a variety of fruits and vegetables, such as cabbage, tea, apple, pear, blueberry, onion [16]. These sources exhibit good medicinal-food homology and have attracted significant research attention. Quercetin has been proven to exert strong anti-fibrosis, antioxidant, anti-inflammatory and other biological activities, which render it to possess a favorable therapeutic potential in ER stress- and ferroptosis-related diseases [17–20]. Additionally, Zhang et al. found that quercetin could inhibit ER stress and improve scleral ECM remodeling by regulating the PERK-EIF2α pathway. However, due to the hydrophobicity of quercetin, dimethyl sulfoxide (DMSO) was used as the solvent for intraperitoneal injection in this experiment, which lead to certain limitations [21]. After being absorbed into the bloodstream, only a small amount of quercetin reaches the eye due to physiological barriers such as metabolic, blood-aqueous, and blood-retinal barriers, resulting in low bioavailability. Moreover, DMSO also has potential toxic effects on cells [22]. Consequently, it is of great significance to innovate safe drug delivery strategies to solve the problems of hydrophobicity and low bioavailability of quercetin, thereby enhancing its therapeutic potential.

Natural nanocarrier exosomes possess excellent biocompatibility, strong biological barrier penetration and low immunogenicity. Notably, these vesicles possess intrinsic targeting abilities, allowing them to deliver drugs effectively to specific cells or tissues while avoiding

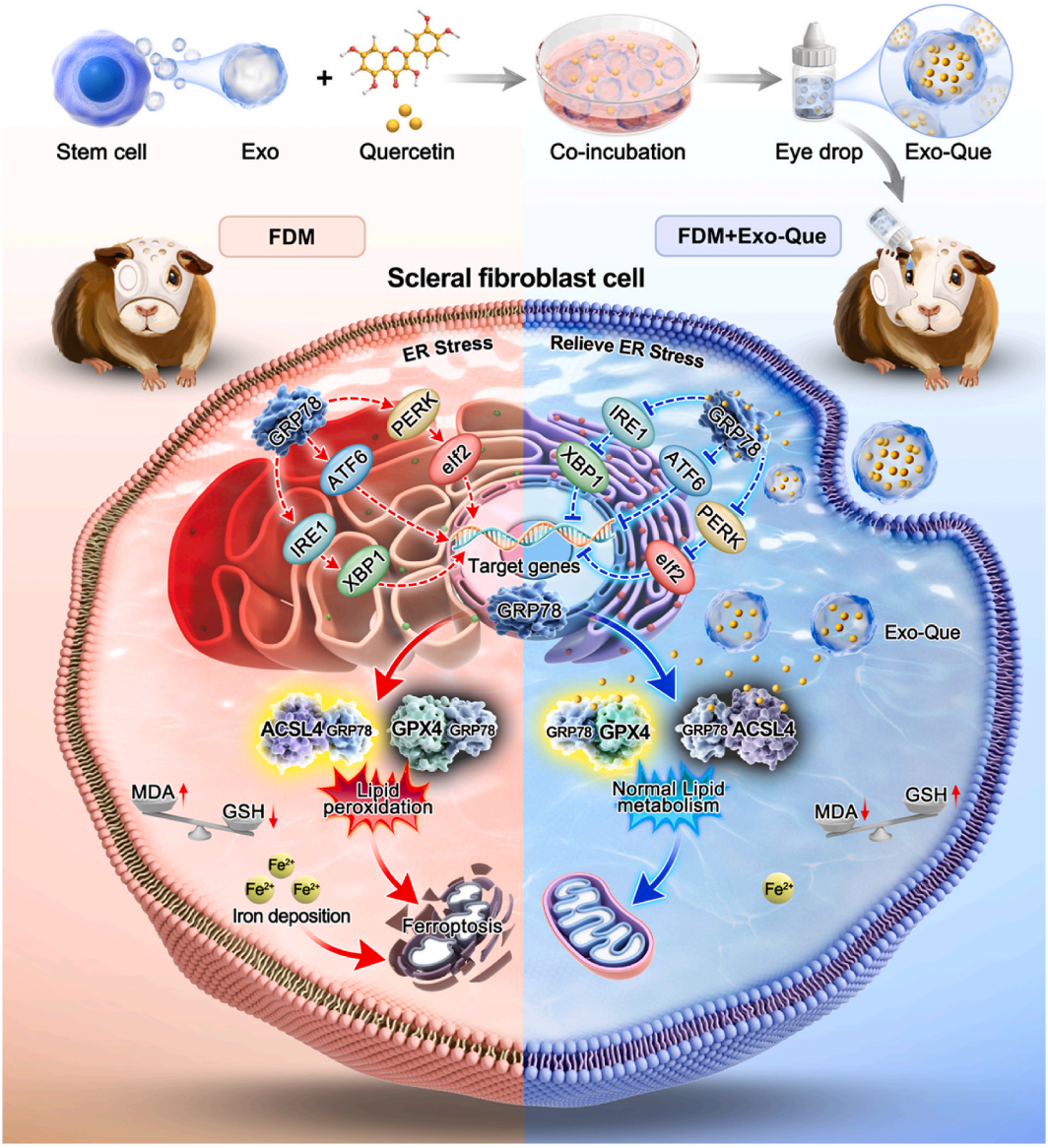

Fig. 1. Schematic illustration of Exo-Que eye drops for myopia prevention.

immune responses and lysosomal degradation. These advantages make exosomes superior to synthetic nanocarriers for drug delivery, particularly in ophthalmic diseases [23,24]. Increasing evidence shows that exosome-based drug delivery systems have achieved favorable therapeutic outcomes in treating ophthalmic disease, including corneal injury, dry eye, vitreoretinal diseases, and choroidal neovascularization [25–32]. Particularly, their ability to traverse biological barriers and distribute extensively in posterior ocular tissues, such as the retina and choroid, enhances their potential for treating myopia. However, there is no report on myopia prevention with exosome-based drug delivery system. It would be intriguing to use such strategies to deliver natural products for the treatment of myopia progression.

In this study, we developed a quercetin-loaded exosomes delivery system (Exo-Que) to improve the bioavailability of quercetin for myopia prevention (Fig. 1). The physical properties, storage stability, cytotoxicity, cellular uptake, and precorneal residue of the fabricated Exo-Que were further evaluated. Subsequently, the effect of Exo-Que on the treatment of myopia was investigated using form-deprivation myopia (FDM) guinea pig model. Additionally, to elucidate the underlying therapeutic mechanisms, we explored the role of ferroptosis in scleral ECM remodeling during myopia progression, and further investigated the effects of quercetin on ferroptosis and ER stress-related pathways. Furthermore, we also assessed the biosafety of Exo-Que, which are expected to provide promising strategies for myopia prevention.

2. Materials and methods

2.1. Materials and reagents

Fetal bovine serum (FBS), penicillin–streptomycin, CCK-8 assay kit, 4′,6-diamidino-2-phenylindole (DAPI), 4 % paraformaldehyde, Triton X-100 and bovine serum albumin were purchased from Servicebio (Wuhan, China). DMEM/F12, fibroblast culture system, and Nuwacell® ncMission hMSC Medium were obtained from Sigma-Aldrich, ICell Bioscience Inc., and Shownin Biotechnologies Co., Ltd., respectively. Quercetin (CAS No.: 117-39-5, purity: 99.8 %) and tunicamycin (CAS No.: 11089-65-9, purity: 99.0 %) were purchased from Med Chem express (Shanghai, China). 1,1′-dioctadecyl-3,3,3′,3′-tetramethylindotricarbocyanine iodide (DiR) and 1,1′-dioctadecyl-3,3,3′,3′-tetramethylindodicarbocyanine perchlorate (DiD) were bought from Macklin Biochemical Co., Ltd. (Shanghai, China). The micro-reduced glutathione (GSH) assay kit, micro-malondialdehyde (MDA) assay kit, and Iron assay kit were bought from Nanjing Jiancheng Bioengineering Institute (Nanjing, China). BCA protein concentration kit, phenylmethylsulfonyl fluoride, protein A + G agarose, and cell lysis buffer for western blotting and immunoprecipitation were purchased from Beyotime Biotech Inc. (Shanghai, China). Capillary western blot reagents were obtained from ProteinSimple (Santa Clara, CA, USA).

2.2. Cell culture

Human umbilical cord-derived mesenchymal stem cells (HUCMSCs), human corneal epithelial cells (HCECs) and human scleral fibroblast cells (HSFCs) were provided by Shenzhen Wingor Biotechnology Co., Ltd. and ICell Bioscience Inc. (Shanghai, China), respectively. All these cells were cultured in growth medium with 10 % FBS and 1 % penicillin-streptomycin as specified by the manufacturers and maintained in an incubator with 5 % CO_2 at 37 °C. The HSFCs were firstly identified by vimentin detection as previously described (Supplementary Fig. S1) [10]. All the three types of cells between 3 and 5 passages were used for the experiments.

2.3. Preparation and characterization of Exo-Que

2.3.1. Exosome extraction

HUCMSCs were plated in serum-free MSC medium and incubated at 37 °C and 5 % CO_2. When the cells reached 90 % confluence, the culture supernatants were collected and subjected sequential to centrifugation at 2000 rpm for 20 min and 12,000 rpm for 30 min at 4 °C to eliminate cellular debris, dead cells, microvesicles, and protein aggregates. Subsequently, the supernatant was then passed through a centrifugal filter unit with a pore size of 0.22 μm to eliminate apoptotic bodies and microvesicles. Then, exosomes were isolated from the cell supernatants using the ultrafast-isolation system (EXODUS) device (Huixin Lifetech, Shenzhen, China) [33]. The obtained exosomes were resuspended in PBS and stored at − 80 °C until further use.

2.3.2. Preparation of Exo-Que

Exo-Que was prepared using a method previously reported by Tao et al., with modifications [28]. Briefly, quercetin was incorporated into DMSO to reach a drug concentration of 1 mg/mL. 1 mL quercetin solution and 9 mL exosomes solution were thoroughly mixed (containing 1.0×10^{12} particles/mL) and incubated at 37 °C for 2 h, facilitating the incorporation of quercetin into the exosomes to form Exo-Que. Subsequently, Exo-Que was isolated from the amalgamated solution by the EXODUS device. Finally, the Exo-Que was resuspended in PBS for eye drop preparation (containing 2.0×10^{10} particles/mL) and stored at −80 °C until further use.

2.3.3. Characterization and stability assessment of Exo-Que

To observed the morphology, 10 μL of exosomes and Exo-Que were placed on a carbon-coated copper grid and stained with 2 % uranyl acetate for 2 min. Then, the exosomes and Exo-Que were air dried and viewed under a transmission electron microscopy (TEM, FEI Tecnai G2 12, USA) at 100 kV. The concentration, zeta potential, and size distribution of exosomes and Exo-Que were examined using nanoparticle tracking analysis (NTA) with ZetaView PMX-120 (Particle Metrix, Germany). Total exosomal protein content was determined using a Qubit protein assay kit (Thermo Fisher, USA), and western blotting was performed to detect the expression of exosomal markers, including CD9 (1:1000, 13174S, Cell Signaling Technology, USA), CD81 (1:1000, sc-166029, Santa Cruz, USA), TSG101 (1:1000, ET1791-59, HUABIO, China), and Alix (1:1000, sc-53540, Santa Cruz, USA). To evaluate the stability of Exo-Que after storage at −80 °C, NTA was used to assess changes in concentration, zeta potential, and size distribution at 15 and 30 days after freezing. Morphological changes were observed by TEM at the same time.

2.3.4. Entrapment efficiency of quercetin and in vitro drug release

The drug loading of Exo-Que was determined using HPLC (Agilent, USA), and the entrapment efficiency was subsequently calculated. To disrupt the Exo-Que membrane structure and release quercetin, 5 mL of methanol was added to 1 mL of Exo-Que. The supernatant was collected after centrifugation at 1000×*g* for 5 min and analyzed by HPLC. During the HPLC analysis, the mobile phase consisted of a 0.1 % methanol aqueous solution-acetonitrile (70:30, v/v) with a flow rate of 0.2 mL/min, and the detection wavelength was set at 370 nm. The entrapment efficiency of quercetin was calculated based on its quantified content. For the *in vitro* sustained-release assessment, a dialysis bag (MWCO 3500 Da) containing 4 mL of Exo-Que was placed in PBS and dialyzed at 37 °C on a constant-temperature water bath shaker. At 30 min, 1 h, 2 h, 4 h, 8 h, 12 h, 24 h, 36 h, and 48 h, 1 mL of dialysate was removed and replaced with an equal volume of fresh PBS. The amount of quercetin released into the dialysate was measured by HPLC, and the cumulative release profile over time was plotted using GraphPad Prism 9.

2.4. In vitro biocompatibility

2.4.1. Cytotoxicity study

The viability and cytotoxicity of HCECs were assessed using a CCK-8 assay kit to evaluate the safety of Exo-Que. HCECs were seeded into 96-well plates at a density of 10000 cells/well and cultured in standard

culture media (DMEM/F12, 10 % FBS, and 1 % antibiotic/antimycotics) for 24 h at 37 °C and 5 % CO_2. The medium was then replaced with 100 μL of DMEM/F12 containing different concentrations of Exo-Que (0, 1.0 × 10^{10} particles/mL, and 2.0 × 10^{10} particles/mL). Cell proliferation was evaluated using a CCK-8 assay after incubation for 12, 24, 36, and 48 h.

2.4.2. In vitro scratch wound assay

The HCECs were plated into 12-well plates at a density of 2 × 10^5 cells/well. The cell monolayer was scratched using a 200 μL pipette tip at 90 % confluence and washed with PBS to remove the damaged cells. Fresh medium containing different concentrations of Exo-Que (0, 1.0 × 10^{10} particles/mL, and 2.0 × 10^{10} particles/mL) was added and co-incubated for 36 h. Photographs of the wound area were captured at 0, 12, 24, and 36 h and analyzed using ImageJ software.

2.5. Fluorescent labeling of Exo-Que

As previously reported [34], DiR and DiD were used to label Exo-Que. In brief, the Exo-Que solution was stained with DiR for 2 h at 37 °C. Excess fluorescent dyes were removed using an ultrafast-isolation system (EXODUS). DiD-labeled Exo-Que solution was prepared using the same method. All DiR-labeled and DiD-labeled Exo-Que solutions were stored at −80 °C until further use.

2.6. Uptake of Exo-Que by HCECs and HSCFs

HCECs and HSCFs were seeded at a density of 1.5 × 10^4 cells/dish into observation dishes, respectively. After adhesion, cells were incubated in medium containing DiD-labeled Exo-Que and fixed at different time points to observe cellular uptake [35]. For confocal analysis, HCECs and HSCFs were washed three times with PBS and fixed with 4 % paraformaldehyde for 30 min. After gently washing, the cells were treated with 0.1 %Triton X-100 for 20 min. The cells were then washed three times and stained using DAPI for 10 min. Ultimately, the cells were observed by a laser scanning confocal microscope (Olympus, Japan).

2.7. In vivo fluorescence imaging of precorneal retention

To evaluate the ocular surface retention of Exo-Que eye drops, 10 μL of free DiR (5 μM) or DiR-labeled Exo-Que was instilled on the ocular surface of guinea pigs after anesthesia, and their head regions were imaged using the IVIS Lumina imaging system (PerkinElmer) at different time points. Data analysis was performed using Living Image software (version 4.5.5). The experiment was repeated three times.

2.8. Animal study

Guinea pigs (tricolor strain, male, 110g–130g) aged 2 weeks were purchased from Jinan Jinfeng Experimental Animal Company and maintained in a 12 h/12 h light/dark cycle environment with suitable temperatures and abundant food. All animal experiments were approved by the Ethics Committee of Shandong University of Traditional Chinese Medicine (Jinan, China, Approval No.: SDUTCM20240306402, March 6, 2024) and conducted following the guidelines outlined in the ARVO Statement for the use of animals in ophthalmic and visual research.

After excluding eye diseases, guinea pigs were randomly divided into five groups: (1) negative control (NC, n = 55), (2) FDM (n = 55), (3) FDM with Exo-Que eye drops (FDM + Exo-Que group, n = 55), (4) FDM with blank exosomes (FDM + Exo group, n = 30), and (5) FDM with 0.1 % atropine eye drops (0.1 % atropine group, n = 30). For the FDM animal model, a 3D-printed removably hood was modified by a latex balloon with 60 % light transmission to cover the right eye of the guinea pig, leaving the ears, left eye, nose, and mouth exposed [36]. The FDM + Exo-Que, FDM + Exo and 0.1 % atropine groups used Exo-Que, blank exosomes and 0.1 % atropine eye drops six times per day (10 μL/time), respectively. At the same time, FDM group only removed and reworn the 3D-hood without eye drops. To minimize any possible effect of light on recovery from FDM, all operations were performed within 10s under dim conditions, and the 3D-hoods were put back instantly once the operation finished.

2.9. Measurement of ocular biometry and refraction

Refraction and ocular biometric parameters were performed before and after 2-week or 4-week treatments. Changes of ocular biological parameters were measured by A-scan ultrasonography (Sunkingdom, China), and refractive errors were measured after cycloplegia using an infrared photorefractor (Striatech GmbH, Germany) in a darkened room. The AL of each eye was repeated for 10 times and refraction was measured 3 times, and the average values were taken as final results.

2.10. Biocompatibility assessment of Exo-Que in vivo

After 4 weeks of intervention, six guinea pigs in each group (NC, FDM, and FDM + Exo-Que) were randomly selected to evaluate corneal health under a slit-lamp microscope, and subsequently euthanized with an intraperitoneal injection of 4 % pentobarbital. Three guinea pigs were randomly selected from each group, and their right eyes and major visceral organs (including the liver, kidney, lung, and heart) were fixed to perform hematoxylin and eosin (H&E) staining for histological observation. Orbital blood samples were taken from all guinea pigs for biochemical examinations.

2.11. TEM of scleral tissue

After 2- and 4-week treatments, three guinea pigs from each group were randomly selected at each time point, and scleral tissues (1 mm^3) were isolated and fixed with TEM fixative for 48 h at 4 °C, then post-fixed with 1 % osmium for 2 h at room temperature, protected from light. After dehydration, tissues were embedded in an epoxy resin mixture at 60 °C for 48 h and sliced into 50–60 nm sections for TEM examination (HT7800, Hitachi, Japan). Before ultrastructure observation, all sections were stained with 2 % uranium acetate saturated alcohol solution to avoid light staining for 10 min, and then 2.6 % lead citrate avoid CO_2 staining for 10 min.

2.12. Iron, GSH and MDA assay

Iron, GSH, and MDA assay kits were used to measure the contents of iron, GSH, and MDA in scleral tissue, respectively. According to the instructions of reagents, reagent was added into 20 mg of scleral tissue, then the tissue was homogenized and centrifuged to collect the supernatants. Subsequently, supernatants were reacted with working reagents and transferred to 96-well plates, which absorbances at 520 nm, 405 nm and 532 nm were measured by ultraviolet spectrophotometer to calculate the concentration of iron, GSH and MDA.

2.13. Western blot analysis

The relative protein levels of GRP78, PERK, ATF6, eIF2, p-eIF2, IRE1, XBP1, ACSL4, GPX4, CHOP, TGF-β1, MMP2, a-SMA and β-actin were evaluated using the Protein Simple Abby capillary western blotting analyzer (Protein Simple, CA, USA). Three scleral tissue samples per group were randomly selected for protein extraction. Protease inhibitor, phosphatase inhibitor, and RIPA lysis buffer (100 μL:10 mg) were added to scleral tissue, which was thoroughly ground at 4 °C and centrifuged at 10,000 rpm for 5 min. Subsequently, the supernatants were collected, and protein concentrations were measured using a BCA protein concentration kit. The final protein concentration used was 2.5 μg/μL. Primary antibodies used were: GRP78 (1:100; 11587-1-AP, Proteintech Bio, China), IRE1 (1:25; 27528-1-AP, Proteintech Bio, China), PERK

(1:25; 24390-1-AP, Proteintech Bio, China), p-eIF2 (1:50; 11170-1-AP, Proteintech Bio, China), eIF2 (1:250; 28740-1-AP, Proteintech Bio, China), XBP1 (1:50; 24868-1-AP, Proteintech Bio, China), GPX4 (1:50; 67763-1-AP, Proteintech Bio, China), ACSL4 (1:100; 22401-1-AP, Proteintech Bio, China), CHOP (1:25; AF6277, Affinity Bio, China), ATF6 (1:25; DF6009, Affinity Bio, China), MMP2 (1:50; AF5330, Affinity Bio, China), TGF-β1 (1:25; BF8012, Affinity Bio, China), a-SMA (1:50; 19245t, CST, USA) and β-actin (1:250; 66009-1-lg, Proteintech Bio, China). Quantitative analysis of the bands was performed using Compass software (version 6.1.0).

2.14. Real-time PCR

After 2 and 4 weeks of intervention, three guinea pigs in each group were randomly selected for PCR analysis. Total RNA was isolated from scleral tissues using Trizol (Thermo Fisher Scientific, USA). cDNA was synthesized using HiScript II QRT SuperMix for quantitative polymerase chain reaction. qPCR was performed on cDNA using Hieff qPCR SYBR Green Master Mix on a StepOnePlus Real-Time PCR System. The primer sequences were as follows: guinea pig actin forward: GTGGATCAGCAAGCAGGAGT, reverse: CTGTCACCTTCACCGTTCCA; guinea pig eIF2 forward: TCAGAATATGAAATCACAGCCAGGA, reverse: GGTGCCACATCTGGAGTCTTG; guinea pig GPX4 forward: AACCAGTTCGGGAAGCAGGA, reverse: GTGGGCGTCATCTCCATTCA; guinea pig GRP78 forward: ACATGGACCTGTTCCGCTCTAC, reverse: GCCTCATCTGGGTTTATGCCTC; guinea pig CHOP forward: GCCTTTCTCCTTCGGGACACT, reverse: TCCTCAGTCAGCCACGCAAG; guinea pig IRE1 forward: GGCTTGACGAAACTTCCCTT, reverse: CAAAGTCTGCTGCTTCTCACC; guinea pig PERK forward: CTGCAATTATGCCATCAAGAGGA, reverse: TCGTCTTTCAGCCAGATTTCAT; guinea pig ACSL4 forward: GACCAGAGAAGTCCTAAGTGAAGAA, reverse: CCTGGTCTCACAGAAAATAGCAAC; guinea pig ATF6 forward: CCAGAGGCTTAAAGTTCCCAGTC, reverse: GCCTCCTTTGATTTGCAGTGTTC; guinea pig XBP1 forward: GTGGATT CTGATGGCATTGACTC, reverse: GACATTTGAAGAACATGACTGGGT.

2.15. Molecular docking and protein–protein interaction networks

Interactions between quercetin and target proteins, including GRP78, PERK, ATF6, IRE1, ACSL4 and GPX4, were conducted in MOE 2019.01. The structure of quercetin was downloaded from Pubchem (https://pubchem.ncbi.nlm.nih.gov/). The predicted structure of ACSL4 was generated by Alphafold (https://alphafold.ebi.ac.uk/) and those of the other proteins were downloaded from Protein Data Bank (https://www.rcsb.org/). Before docking, the proteins were edited to remove water molecules and add hydrogen atoms. The activity of the ligand for a specific receptor was assed using an S-score.

Protein-protein interaction network was built through the STRING database (http://string-db.org/), with species limited to *Homo sapiens*. The confidence score was set to >0.4 (medium confidence). Protein-protein docking was predicted by AutoDock 1.5.7. To ensure the accuracy of the docking results, proteins and the resulting protein-protein complex were all edited to remove all water molecules and add hydrogen atoms. Finally, protein-protein interactions were predicted, and the interaction figure was generated by PyMOL.

2.16. Co-immunoprecipitation (Co-IP) assay

To identify the interaction of GRP78 with ACSL4 and GRP78 with GPX4, Co-IP was performed in HSFCs ER stress model and FDM guinea pig sclera tissue. In brief, HSCFs were treated with 200 ng/mL tunicamycin for 24 h to induce ER stress model when the cells reached 80 % confluence [9]. Then, the cells were collected and lysed within 200 μL cell lysis buffer for western blotting and immunoprecipitation containing 1 × protease inhibitor cocktail for 20 min on ice. The supernatant with protein were obtained by centrifugation at 10,000 rpm for 15 min at 4 °C. Protein concentration was determined using the BCA kit. One-tenth volume of supernatant with protein was taken out as input, and the remaining portion was mixed with 50 μL of protein A + G agarose for 1 h at 4 °C to reduce non-specific binding and background. Subsequently, the supernatant with protein was mixed with GRP78 (1:100; 11587-1-AP, Proteintech Bio, China) or ACSL4 (1:50; sc-365230; Santa Cruz, America) or GPX4 (1:50; sc-166570; Santa Cruz, America) respectively, as the bait protein, at 4 °C overnight. The incubation was sustained for 3 h, followed by the addition of protein A + G agarose. The immunocomplexes were washed 4 times by PBS supplemented with protease inhibitor. Finally, western blot analysis was performed with ACSL4 or GPX4 or GRP78, as the prey protein. IgG (1:50; AC005, ABclonal, China) was used as the protein loading control. All the biological replicates for western blots were three (n = 3).

2.17. Immunofluorescence staining

Immunofluorescence intensity was used to analyze the co-localization of GRP78 with GPX4 or ACSL4 in the scleral tissues and HSCFs. Briefly, HSCFs were seeded in a 12-well plate containing slides and co-incubated with tunicamycin (200 ng/mL) or tunicamycin (200 ng/mL) and Exo-Que (2.0×10^{10} particles/mL) for 24 h. The cells were then fixed with 4 % paraformaldehyde for 30 min, permeabilized with 0.1 % Triton X-100 for 15 min, and blocked with 10 % BSA for 1 h at 37 °C. Subsequently, the cells were incubated with particular primary antibodies, GRP78 (1:50; 11587-1-AP, Proteintech Bio, China) and GPX4 (1:50; 67763-1-AP, Proteintech Bio, China) or GRP78 (1:50; 11587-1-AP, Proteintech Bio, China) and ACSL4 (1:50; sc-365230, Santa Cruz, America) overnight at 4 °C. After washing, the cells were incubated with a fluorescent secondary antibody for 1 h at 37 °C (in the dark). Finally, the cells were stained using DAPI for 10 min and observed by a laser scanning confocal microscope (Olympus, Japan). The immunofluorescence staining of scleral tissues were performed using the similar method. The co-localization analysis was carried out using the Image J software. All experiments were repeated for three iterations to ensure the authenticity and reliability of the results.

2.18. Statistical analysis

Statistical analyses were performed using SPSS version 24.0. Quantitative data are expressed as mean ± standard deviation. The Shapiro-Wilk normality test was used to analyze the distribution of all datasets. One-way ANOVA was used to assess the differences among different groups for normally distributed data, whereas the Kruskal-Wallis non-parametric test was utilized for non-normally distributed data. The intensity of co-localization was quantified using the Pearson correlation coefficient. P-value <0.05 was considered statistically significant.

3. Results

3.1. Preparation and characterization of Exo-Que

Although quercetin exhibits certain efficacy in controlling myopia progression, its therapeutic potential remains unclear. Moreover, its hydrophobic nature and interference from ocular physicochemical barriers reduce its bioavailability for *in vivo* applications. In this study, we prepared a novel quercetin delivery system, which was referred to as Exo-Que, aiming to improve the bioavailability of quercetin (Fig. 2A). Firstly, we identified the exosomes which were isolated from the supernatants of cultured HUCMSCs. TEM observation showed that the exosomes had a cup-like appearance (Fig. 2B). Importantly, exosome markers, including CD9, CD81, TSG101 and ALIX, were successfully detected by western blotting (Fig. 2C). NTA revealed that the exosomes had an average diameter of 125.87 ± 21.32 nm and an average zeta potential of −44.22 ± 2.08 mV (Fig. 2D and E). All these results verified that we had successfully extracted exosomes.

Subsequently, we used the co-incubation method to prepare Exo-Que

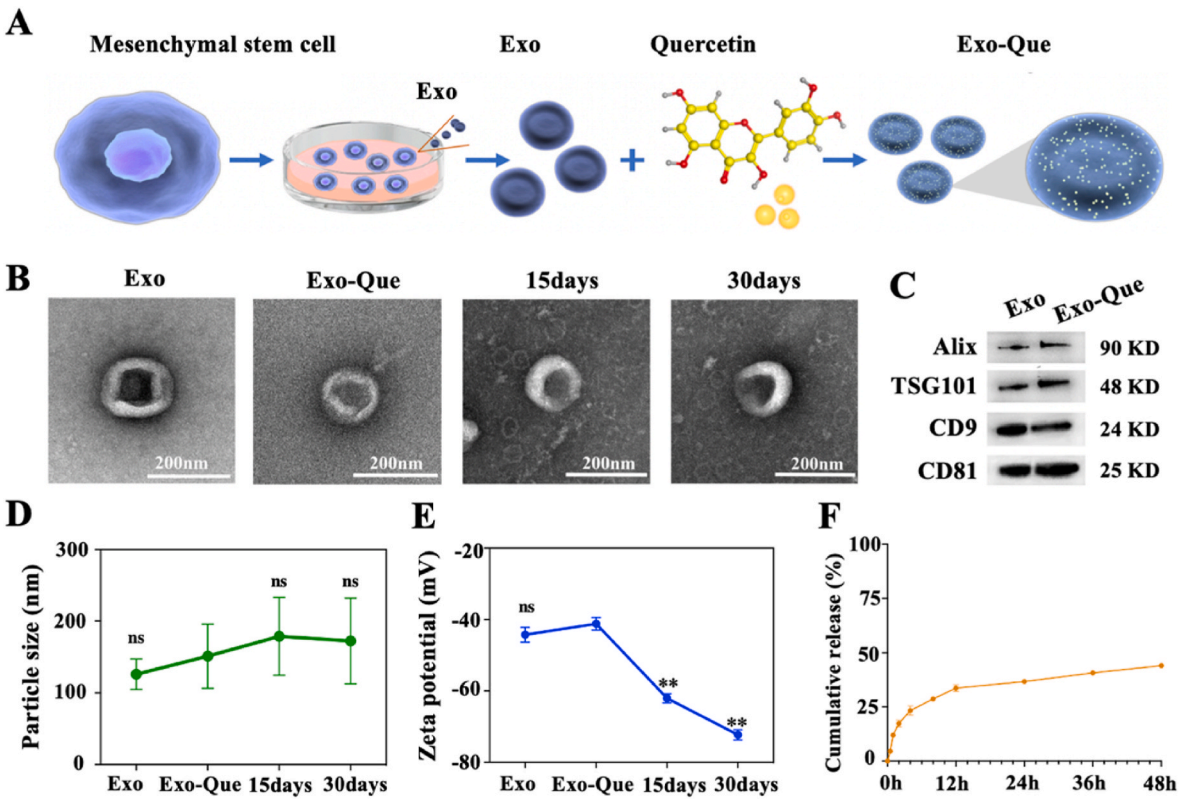

Fig. 2. Construction and characterization of Exo-Que. (A) Synthetic reaction; (B) TEM images of Exo-Que in different states; (C) Western blotting analysis of Exo-Que using exosome markers including ALIX, TSG101, CD9 and CD81; (D, E) Particle size and Zeta potential of Exo-Que; (F) In vitro release profiles of the Exo-Que.**$p < 0.01$, p-values represent the statistical comparisons before and after drug loading, as well as before and after cryopreservation.

and evaluated its preparation feasibility, physical characterization, and storage stability. As expected, Exo-Que maintained the cup-like morphology with an average diameter of 151.13 ± 44.82 nm and an average zeta potential of −41.17 ± 1.75 mV. The marker protein identification results were consistent with those observed before drug loading (Fig. 2B–E). This indicated that the drug-loading process did not destroy the unique morphological structure and properties of exosomes. Furthermore, the drug entrapment efficiency of Exo-Que was 20.15 ± 1.10 %. In vitro release profile of Exo-Que at predetermined time points was presented in Fig. 2F. Approximately 4.57 % and 23.33 % of quercetin were rapidly released from Exo-Que within the first 30 min and 4 h, respectively. At 24 and 48 h, the cumulative release of quercetin reached approximately 36.67 % and 44.01 %, respectively. All these results clearly demonstrated the sustained-release characteristics of Exo-Que. Additionally, storage stability evaluations of Exo-Que at −80 °C for 15 and 30 days revealed that the morphology of Exo-Que did not change significantly after cryostorage. NTA results showed that the average diameter of Exo-Que after 15 and 30 days of freezing was 178.90 ± 57.29 nm and 172.53 ± 77.01 nm, respectively, with no significant differences compared to pre-freezing values ($p > 0.05$). The zeta potential became −62.04 ± 0.86 mV and −72.32 ± 1.41 mV, which was lower than before, but still within the normal range (Fig. 2D and E). In summary, Exo-Que is an ideal drug delivery system with good storage stability.

Good biocompatibility and low cytotoxicity are essential for *in vivo* applications. To assess whether Exo-Que possesses these properties, we proceeded to evaluate its *in vitro* performance. CCK-8 and scratch wound assays confirmed that Exo-Que had no toxic effect on the proliferation and migration ability of HCECs (Fig. 3A). Interestingly, the high concentration of Exo-Que (2.0×10^{10} particles/mL) promoted scratch wound healing at 24 h (Fig. 3B and C), indicating that Exo-Que is a safe drug delivery system.

Additionally, enhancing drug permeability and extending the ocular surface residence time constitute crucial strategies for improving drug bioavailability. To assess the uptake of Exo-Que by HCECs and HSFCs, the fluorescent probe DiD was encapsulated into Exo-Que for fluorescence tracing. As depicted in Fig. 3D, the red fluorescence from DiD-labeled Exo-Que accumulated around the perinuclear region (blue fluorescence) in both HCECs and HSFCs, which gradually intensified with the extension of incubation time. The cellular internalization was nearly complete within 15–30 min, suggesting excellent cell permeability of Exo-Que. Subsequently, we used *in vivo* fluorescence imaging system to assess the precorneal retention of Exo-Que. Results demonstrated that the fluorescence intensity of free DiR group decreased rapidly, which retained about 54 % within 10 min and 30 % within 40 min, validating the rapid precorneal elimination. While the DiR-labeled Exo-Que exhibited good precorneal retention ability, with a fluorescence intensity of approximately 90 % within 10 min and 74 % after 40 min (Fig. 3E and F). Overall, the high cellular uptake and prolonged retention time of Exo-Que provide adequate quercetin bioavailability. These characteristics are reflective of a promising drug delivery system.

3.2. *Prevention efficacy of Exo-Que in the FDM Guinea pig model*

Encouraged by the advantages of Exo-Que, we evaluated its efficacy in preventing myopia in FDM guinea pigs. We first established FDM models and administered Exo-Que drops (Fig. 4A). After two and four weeks of treatment, the refraction in the NC groups was 0.67 ± 0.92 D and −0.24 ± 0.60 D, respectively. While form-deprivation induced significant myopic in both the FDM group (−1.84 ± 1.07 D at two weeks and −4.84 ± 1.26 D at four weeks) and the FDM + Exo group (−1.96 ± 1.02 D at two weeks and −4.50 ± 1.20 D at four weeks). Conversely, the FDM + Exo-Que group did not show significant myopia at two and four weeks (0.80 ± 0.95 D at two weeks and −0.33 ± 0.63 D at four weeks)

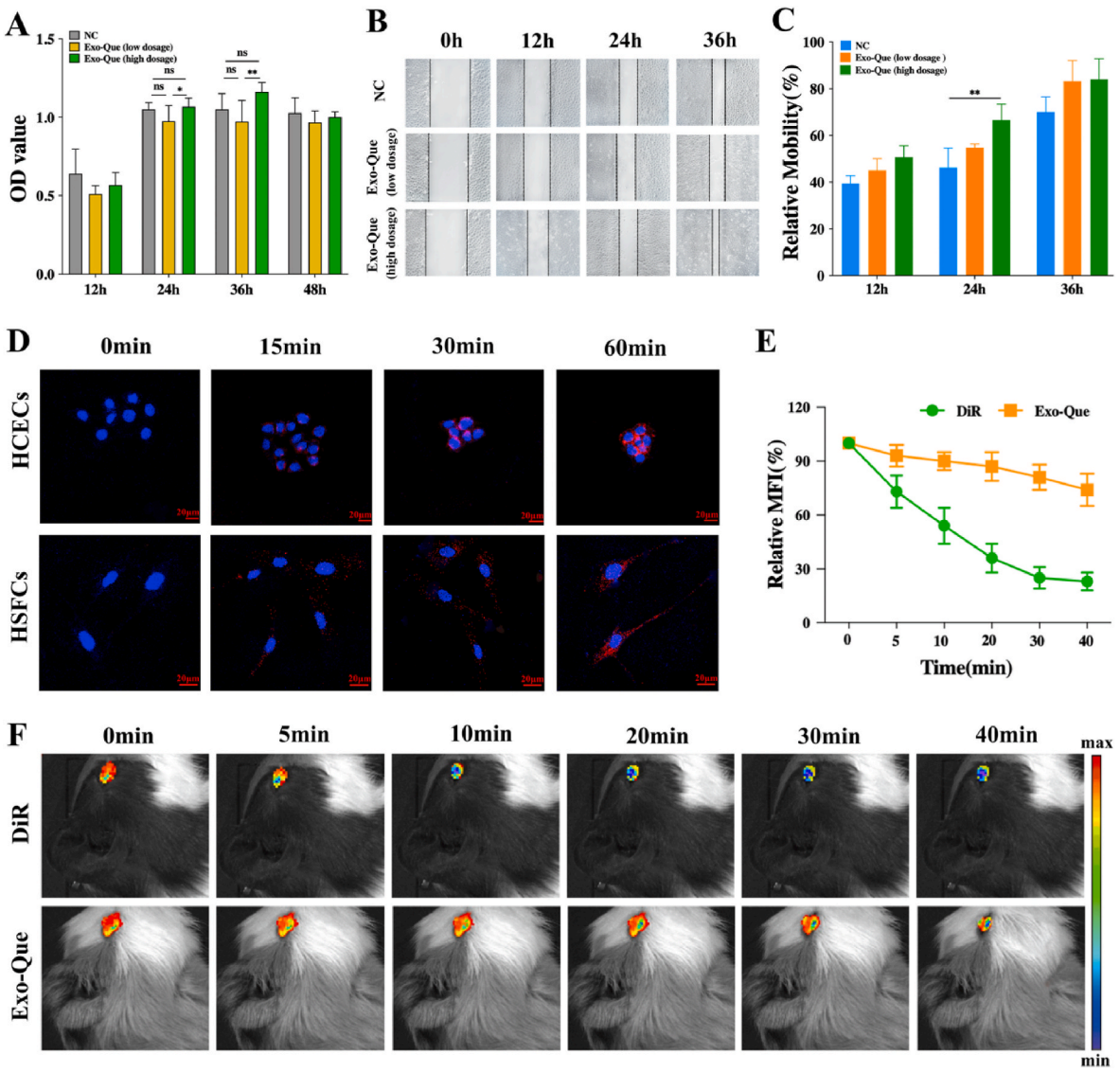

Fig. 3. Evaluation on cytotoxicity, cellular uptake, and precorneal residue of Exo-Que. (A) Quantification of HCECs viability; and (B, C) Migration ability after treatments with PBS, Exo-Que (1.0×10^{10} particles/mL), and Exo-Que (2.0×10^{10} particles/mL); (D) Cellular uptake of DiD-labeled Exo-Que by HCECs and HSFCs. Scale bar: 20 μm; (E, F) Representative *in vivo* fluorescence images of guinea pig eyes after administration of free DiR or DiR-labeled Exo-Que, and quantification of fluorescence signals from free DiR or DiR-labeled Exo-Que (n = 3).

(Fig. 4B). At the same time, the ALs of guinea pigs in the FDM and FDM + Exo groups were significantly extended compared to that in the NC group (at two weeks, NC vs. FDM: 8.04 ± 0.05 mm vs. 8.21 ± 0.07 mm, $p < 0.001$; NC vs. FDM + Exo: 8.04 ± 0.05 mm vs. 8.20 ± 0.06 mm, $p < 0.001$; at four weeks, NC vs. FDM: 8.15 ± 0.07 mm vs. 8.35 ± 0.09 mm, $p < 0.001$; NC vs. FDM + Exo: 8.15 ± 0.07 mm vs. 8.36 ± 0.08 mm, $p < 0.001$). However, Exo-Que significantly inhibited AL elongation (at two weeks, FDM + Exo-Que vs. FDM: 8.06 ± 0.08 mm vs. 8.21 ± 0.07 mm, $p < 0.001$; at four weeks, FDM + Exo-Que vs. FDM: 8.16 ± 0.07 mm vs. 8.35 ± 0.09 mm, $p < 0.001$) (Fig. 4C). Additionally, no significant differences in AL or refraction were observed between the FDM + Exo and FDM groups ($p > 0.05$). This confirms that blank exosomes exert no therapeutic effect in preventing myopia progression, and the observed therapeutic outcomes are attributable to quercetin.

In order to quantify the myopia-controlling effect of Exo-Que, we used atropine as a positive control. Compared with the FDM group, Exo-Que and 0.1 % atropine reduced the myopic refractive error by 58.41 % and 59.07 % at 2 weeks, 59.97 % and 59.84 % at 4 weeks, respectively. The axial length was reduced by 38.46 % and 35.90 % at 2 weeks, 35.85 % and 37.74 % at 4 weeks, respectively (Fig. 4B and C). These data demonstrated that the Exo-Que was comparable to atropine in inhibiting the progression of myopic refractive error and AL, making it an effective strategy for myopia treatment.

3.3. *Exo-Que targeted ER stress and ferroptosis to inhibit scleral ECM remodeling in myopic eyes*

To explore the potential mechanism underlying both the pathogenesis and treatment of myopia, we observed the ultrastructural changes in scleral fibroblasts using TEM. After two weeks of treatment, the sclera ER of guinea pigs in FDM and FDM + Exo group exhibited swelling and distension, while the mitochondria showed signs of shrinkage and a reduction in cristae. By four weeks, the ER in these groups was markedly distended and ruptured, with mitochondrial cristae either lysed or absent, and outer mitochondrial membranes ruptured. Inversely, the morphologies of the ER and mitochondria in the Exo-Que-treated and NC groups were normal (Fig. 5A and B). Further detection showed that the GSH level was decreased, while MDA and iron level were significantly increased in sclera tissues of FDM and FDM + Exo groups. In contrast, Exo-Que treatment reversed the changes of GSH, MDA and iron

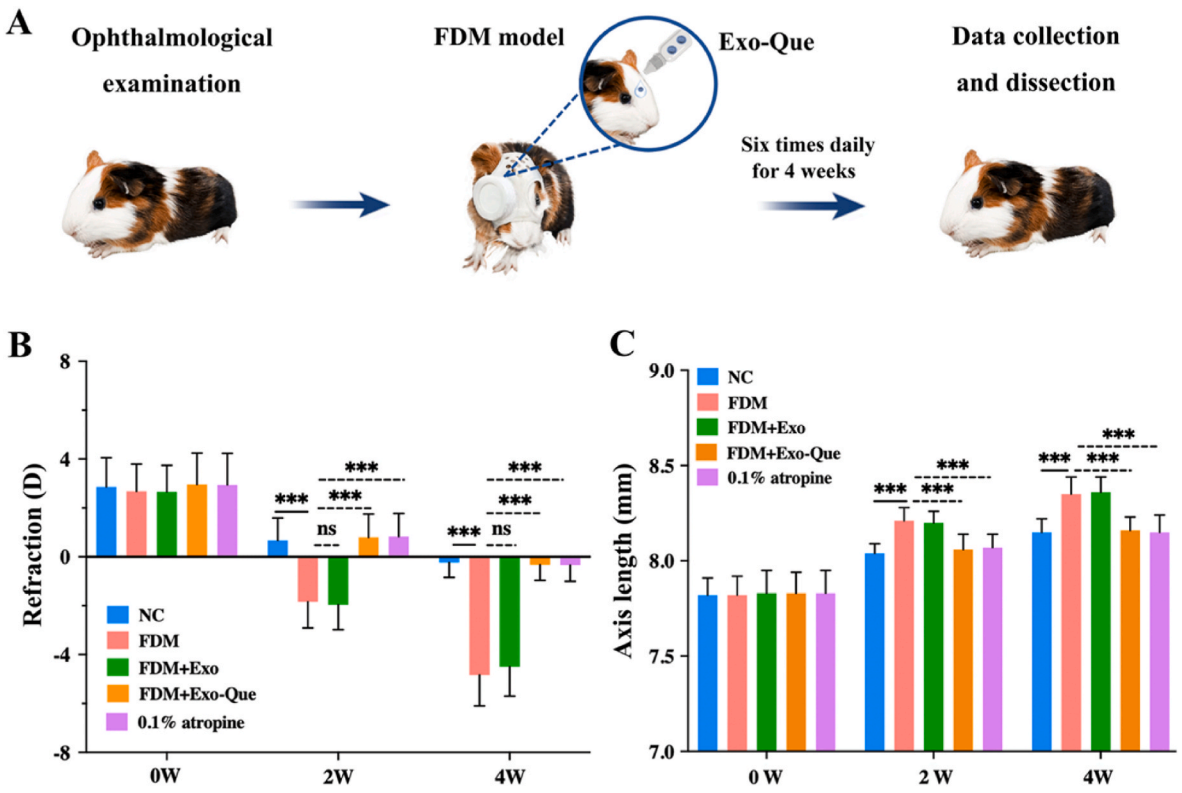

Fig. 4. Preventive effect of Exo-Que on myopia. (A) Schematic indicating the experimental design for evaluating the prevention effect of Exo-Que eye drops in the FDM guinea pig model; (B) Refraction and (C) axial length of the control, FDM, FDM + Exo, FDM + Exo-Que and 0.1 % atropine groups (n = 40 in Control, FDM and FDM + Exo-Que groups; n = 30 in FDM + Exo and 0.1 % atropine groups). ***p < 0.001.

(Fig. 5C). Together, these data confirm that ferroptosis, together with ER stress, were involved in myopia development and Exo-Que could negatively regulate both ferroptosis and ER stress in scleral fibroblasts. The therapeutic efficacy of Exo-Que was primarily attributed to quercetin, rather than the blank exosomes serving as a vehicle.

Given the complexity of the mechanisms of ER stress and ferroptosis, it is crucial to identify the molecules involved in both myopia pathogenesis and Exo-Que treatment. We used western blotting and qPCR to assess the protein and mRNA expressions of ER stress-related and ferroptosis-related markers. Western blot analysis demonstrated that 2- and 4-week of FD activated IRE1-XBP1, PERK-eIF2 and ATF6 pathways, leading to XBP1 activation and eIF2 phosphorylation. Simultaneously, the expression levels of GRP78, CHOP, and the ferroptosis-related protein ACSL4 increased, while the expression of GPX4 decreased. Conversely, Exo-Que inhibited the activation of IRE1-XBP1, PERK-eIF2 and ATF6 pathways, and reversed the expression levels of ferroptosis-related proteins ACSL4 and GPX4 (Fig. 5D–G). qPCR data further revealed that the mRNA expression levels of GRP78, PERK, ATF6, IRE1, XBP1, ACSL4, and CHOP were significantly elevated, while GPX4 mRNA expression was reduced (Fig. 5H and I). In summary, these data further verified that the three major effector pathways of the UPR and ferroptosis-related markers ACSL4 and GPX4 are involved in the onset and progression of myopia, with Exo-Que regulating these signaling molecules to inhibit ER stress and ferroptosis.

To further investigate the effects of ER stress and ferroptosis on the sclera, we examined changes in scleral collagen fibers using TEM and evaluated the expression of matrix remodeling-related proteins, including TGF-β1, MMP2 and a-SMA, in different groups. TEM results confirmed that scleral collagen fibers were thinner and more sparsely arranged in eyes with FDM (Fig. 6A and B). Western blotting demonstrated that the expression level of TGF-β1 was significantly downregulated, while MMP2 and α-SMA levels were significantly upregulated after four weeks of form deprivation (Fig. 6C and D), indicating the transformation of scleral fibroblasts into myofibroblasts and remodeling of the scleral matrix (Fig. 6E). In contrast, the changes were inhibited by Exo-Que (Fig. 6A–D). Taken together, these results suggest that Exo-Que decreases myopia through inhibiting ER stress, ferroptosis and ECM remodeling.

3.4. *Exo-Que targets the protein-protein interaction of GRP78-ACSL4 and GRP78-GPX4 to regulate related signaling pathways*

To investigate potential connections between these signaling molecules, molecular docking and STRING database were used to assess drug-protein and protein-protein interactions. As drug-protein docking results showed that quercetin had strong binding ability to GRP78, ACSL4, and GPX4, with docking scores of −6.62 kcal/mol, −6.55 kcal/mol, and −5.58 kcal/mol, respectively (Fig. 7A–F, Supplementary Fig. S2, and Table S1). Moreover, protein-protein interactions results revealed that the seven proteins, including GRP78, IRE1, XBP1, PERK, eIF2, ATF6 and CHOP, formed one network, while the GRP78, GPX4 and ACSL4 formed another network, indicating the interaction between these proteins (Fig. 8A). Interestingly, GRP78 was the key target linking the two protein interaction networks of ER stress and ferroptosis. Further protein-protein docking predictions confirmed the strong interaction between GRP78 and ACSL4, with multiple residues forming hydrogen bonds or electrostatic interactions, such as the hydrogen bond formed by ALA54 of GRP78 and ASN230 of ACSL4, and the electrostatic interaction formed by ARG49 of GRP78 and GLU252 of ACSL4. Under these interaction forces, the docking score of GRP78-ACSL4 was as high as −646 (Fig. 8B, Supplementary Table S2). Similarly, significant interactions were observed between GRP78 and GPX4 (score: −498), with residues forming hydrogen bonds and electrostatic interactions, such as the hydrogen bond formed by ARG279 of GRP78 and ARG93 of GPX4, and the electrostatic interaction formed by ASP333 of GRP78 and HIS42 of GPX4 (Fig. 8C, Supplementary Table S2).

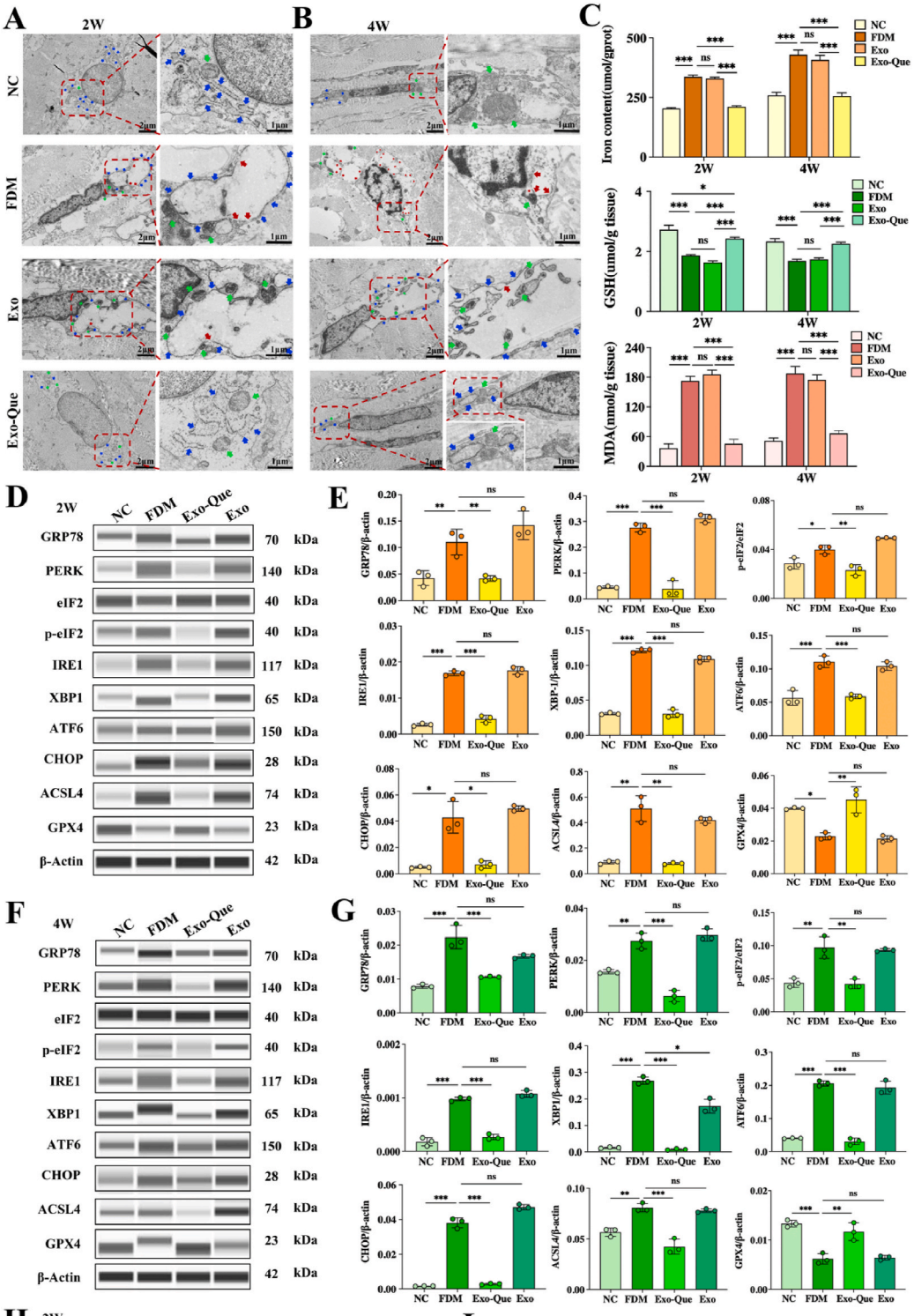

(caption on next page)

Fig. 5. Exo-Que inhibits ER stress and ferroptosis in scleral fibroblasts during myopia progression. (A, B) Morphological changes of scleral ER and mitochondria as detected by transmission electron microscopy in different groups at 2 weeks and 4 weeks (n = 3). Blue arrows indicate the ER, green arrows indicate the mitochondria, and red arrows indicate disruptions of the ER or mitochondria; (C) Quantitative analysis of iron content, MDA level, and GSH level (n = 3); (D–G) Expression levels of ER stress- and ferroptosis-related proteins GRP78, PERK, eIF2, p-eIF2, IRE1, XBP1, ATF6, CHOP, ACSL4, and GPX4 in sclera tissues at 2 and 4 weeks (n = 3 at each time point), *p < 0.05, **p < 0.01, ***p < 0.001; (H and I) The mRNA levels of GRP78, PERK, eIF2, IRE1, XBP1, ATF6, CHOP, ACSL4, and GPX4 were measured by qPCR in the sclera tissues at 2 and 4 weeks (n = 3 at each time point).*p < 0.05, **p < 0.01, ***p < 0.001, p-values represent the statistical comparisons between different groups and the FDM group. (For interpretation of the references to color in this figure legend, the reader is referred to the Web version of this article.)

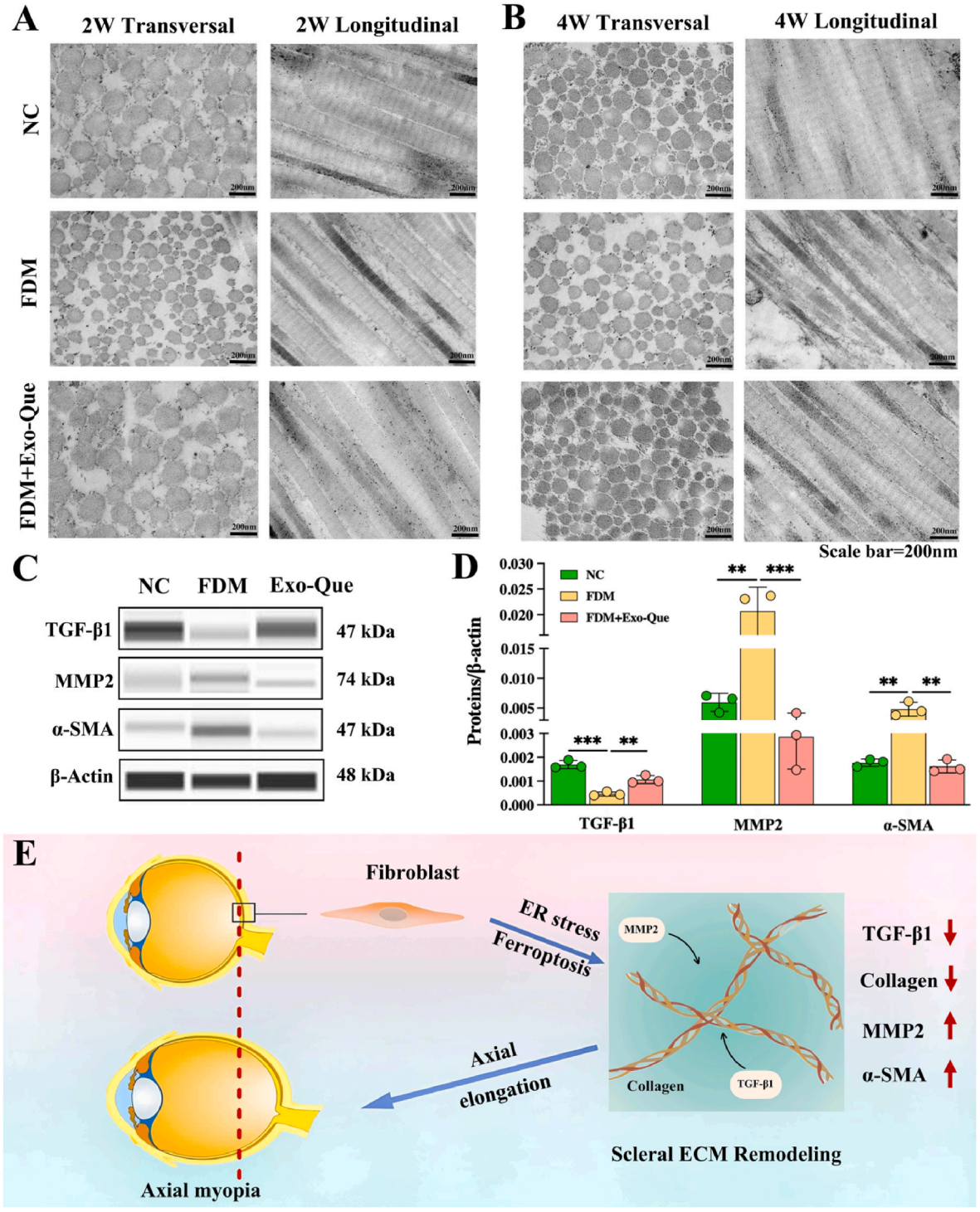

Fig. 6. The elimination of ER stress and ferroptosis alleviates scleral ECM remodeling. (A, B) Transmission electron microscopy images of collagen fibers in scleral tissue at 2 and 4 weeks (n = 3); (C, D) Representative proteins expression of TGF-β1, MMP2 and a-SMA in sclera tissue (n = 3); (E) Schematic illustration of ECM remodeling during myopia progression. **p < 0.01, ***p < 0.001.

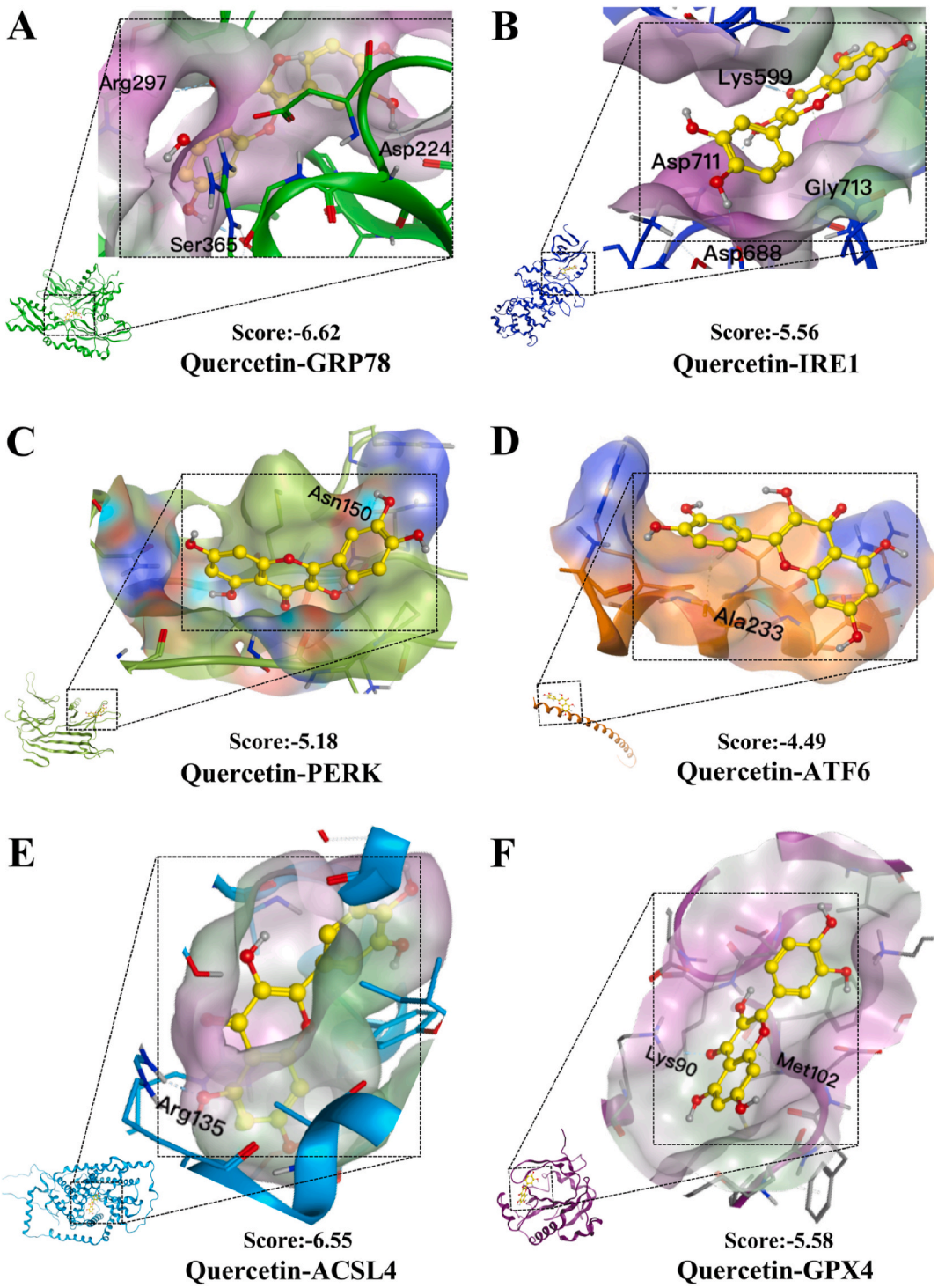

Fig. 7. 3D interaction diagrams of protein binding simulations involving quercetin binding to GRP78, IRE1, PERK, ATF6, ACSL4 and GPX4. (A) GRP78; (B) IRE1; (C) PERK; (D) ATF6; (E) ACSL4; (F) GPX4. Residues are annotated with their 3-letter amino acid code.

Encouraged by the molecular docking predictions, we used Co-IP assay to verify that these protein-protein interactions were really existing during myopia progression. As anticipated, we successfully captured GPX4 and ACSL4 using GRP78 as the bait protein (Fig. 8D). Satisfyingly, GRP78 was also captured in reciprocal Co-IP assay using GPX4 and ACSL4 as bait proteins, respectively (Fig. 8E and F). Given that the ER and mitochondria are common organelles in vertebrates, we used HSCFs to determine whether the GRP78-ACSL4 and GRP78-GPX4 protein interactions are highly conserved across species. We first used tunicamycin to induce ER stress in HSCFs and then carried out Co-IP and reciprocal Co-IP assay. Consistent with that in FDM guinea pig model (Fig. 8G–I), the results provided evidence that strong protein interactions exist among GRP78-ACSL4 and GRP78-GPX4.

Combined with the molecular docking results showing the interaction of quercetin with GRP78, ACSL4, and GPX4, as well as changes in the expression of these proteins following Exo-Que treatment, we hypothesize that the protein-protein interaction among GRP78-ACSL4 and GRP78-GPX4 arrive the targets for quercetin to regulate ferroptosis. To

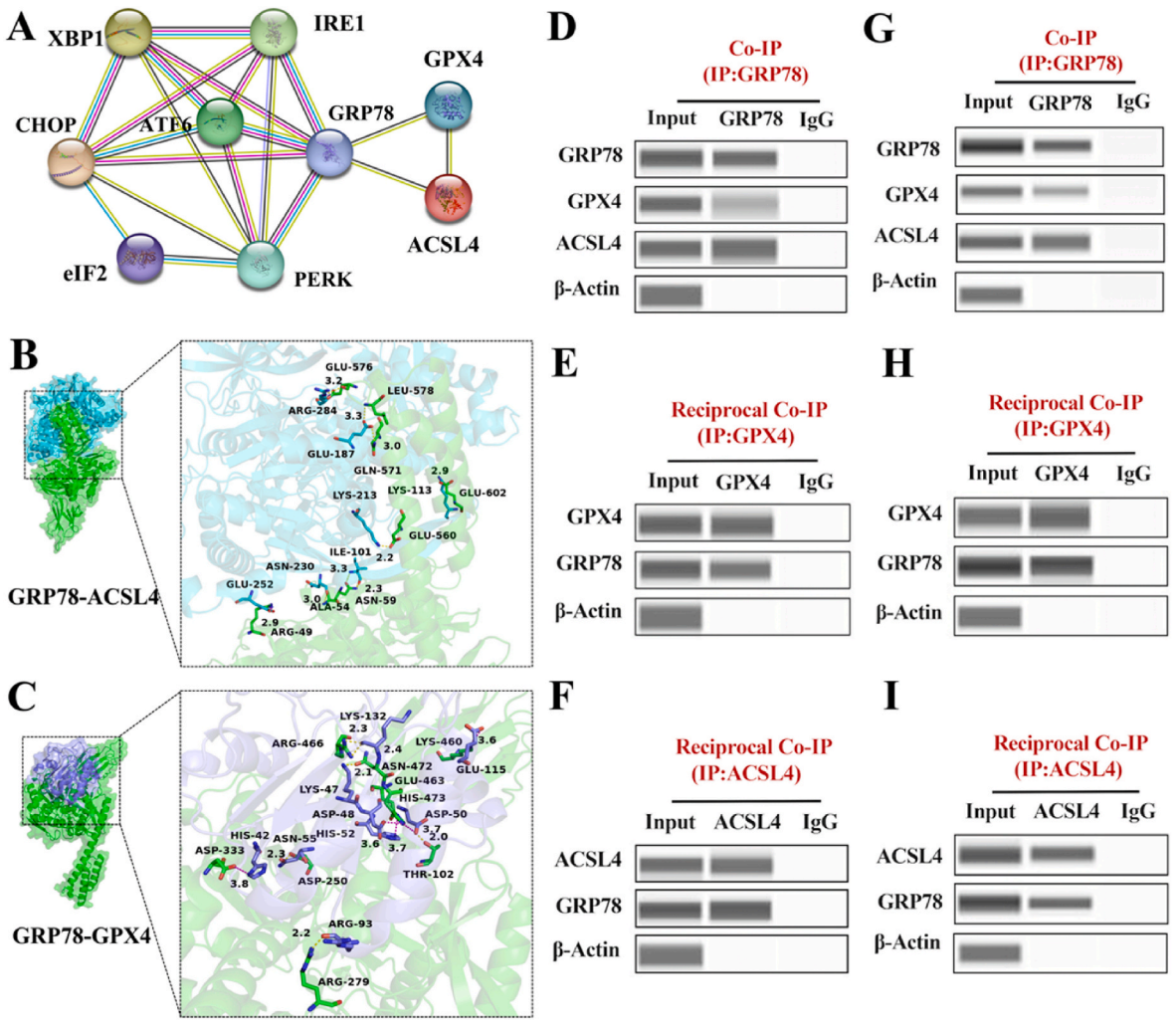

Fig. 8. The protein-protein interaction of GRP78-ACSL4 and GRP78-GPX4. (A) Protein-protein interaction network analysis; (B) Interaction between GRP78 and ACSL4; (C) Interaction between GRP78 and GPX4; (D) Co-IP and (E) reciprocal Co-IP indicate the interactions between GRP78 and ACSL4 in FDM guinea pig model; (D) Co-IP and (F) reciprocal Co-IP indicate the interactions between GRP78 and GPX4 in FDM guinea pig model; (G) Co-IP and (H) reciprocal Co-IP indicate the interactions between GRP78 and ACSL4 in cellular ER stress model; (G) Co-IP and (I) reciprocal Co-IP indicate the interactions between GRP78 and GPX4 in cellular ER stress model.

validate our hypothesis and visualize the protein interactions among GRP78-ACSL4 and GRP78-GPX4 in scleral tissue and HSCFs, we conducted immunofluorescence co-localization labeling and confocal analysis using the FDM guinea pig model and the HSFCs ER stress model. Furthermore, the effects of Exo-Que on the co-localization among GRP78-ACSL4 and GRP78-GPX4 were investigated. Co-localization results demonstrated that GRP78 and ACSL4 exhibited significant co-localization in the scleral tissue of myopic animals (PCC = 0.85) and in the HSCFs ER stress model (PCC = 0.80). Whereas Exo-Que treatment could effectively reduce this co-localization (PCC = 0.69 in animal tissue and PCC = 0.66 in the cell model) (Fig. 9A and C). Additionally, GRP78 and GPX4 also showed co-localization in both the scleral tissue of myopic animals and the HSCFs ER stress model (PCC = 0.61 and 0.79, respectively), which was enhanced by Exo-Que intervention (PCC = 0.75 in animal tissue and PCC = 0.88 in the cell model) (Fig. 9B and D). These findings confirmed that Exo-Que regulates the interactions among GRP78-ACSL4 and GRP78-GPX4.

3.5. *In vivo biosafety evaluation of Exo-Que*

Given the favorable therapeutic effects of Exo-Que, evaluating its biosafety for future clinical applications is crucial. In this study, we evaluated the *in vivo* biocompatibility of Exo-Que through corneal examination, histomorphological assessment (H&E staining), and blood biochemical test. After 4 weeks of Exo-Que administration, no evidence of corneal inflammation, neovascularization, opacity, or conjunctival hyperemia was observed in the FDM + Exo-Que group (Fig. 10A). Furthermore, H&E staining showed the corneal morphology in all groups was regular, with cells closely and orderly arranged, without observable impairment, inflammatory cells and corneal neovascularization (Fig. 10B). All these results indicate that Exo-Que possess excellent ocular tolerance and can be used as a safe therapeutic agent. Subsequently, we further compared the blood biochemical parameters (liver and renal function) and morphological changes of vital organs under physiological, pathological conditions (FDM) and following Exo-Que administration. H&E staining of the liver, kidney, lung and heart revealed that the tissue morphology in the Exo-Que-treated group was similar to that in the control group, with no obvious inflammatory infiltration or signs of acute or chronic toxicity (Fig. 10C). This indicates that Exo-Que is a selective agent *in-vivo*. Additionally, the liver and kidney function remain within normal ranges, with no significant differences between the groups (Fig. 10D). In conclusion, Exo-Que demonstrates no toxic effects and exhibits high biocompatibility, providing a solid foundation for future clinical trials.

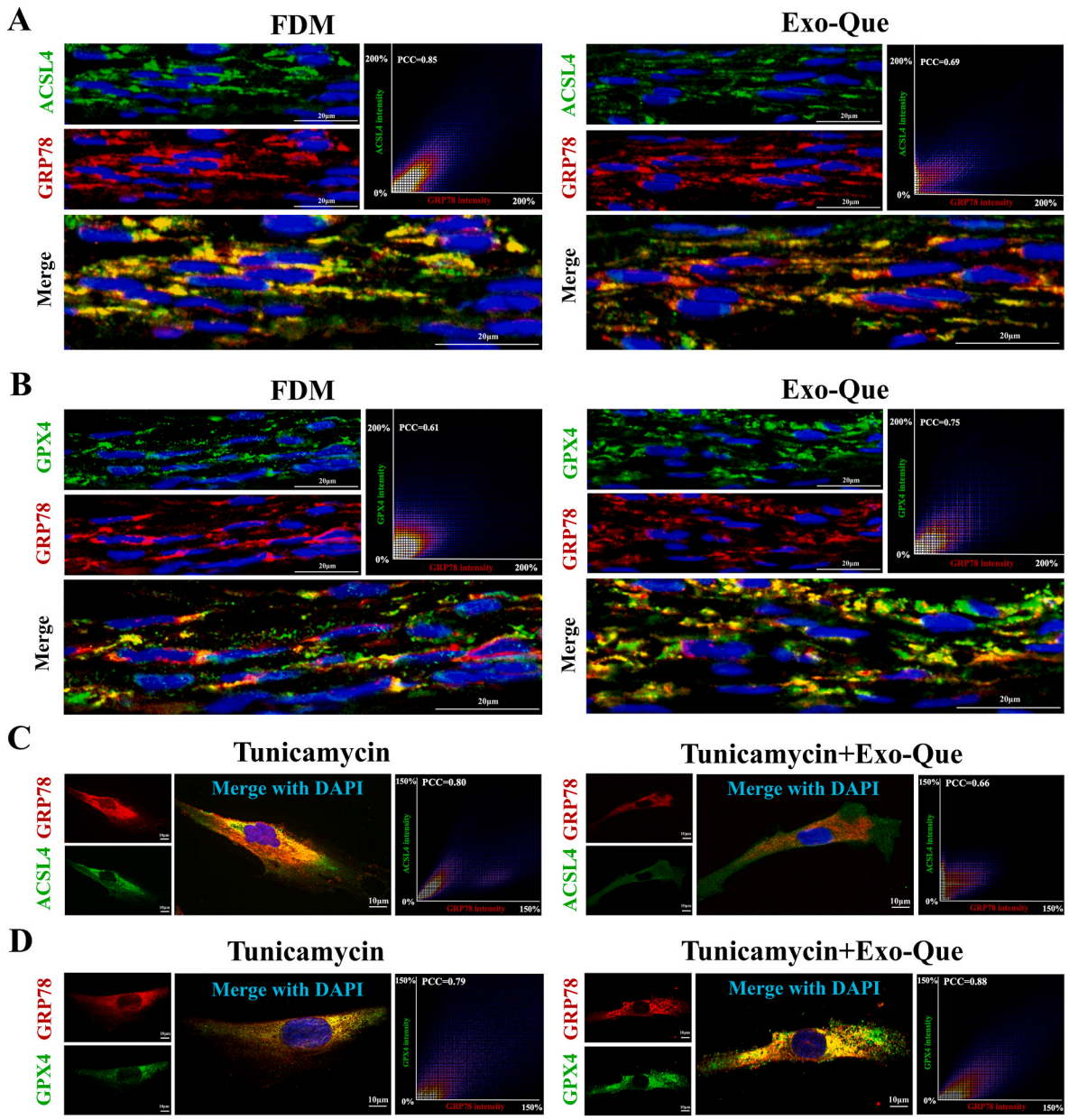

Fig. 9. Exo-Que negatively regulate the interactions of GRP78-ACSL4 and GRP78-GPX4. (A, B) Representative co-localization images of GRP78-ACSL4 and GRP78-GPX4 in the scleral tissue (n = 3), Scale bar: 20 μm; (C, D) Representative co-localization images of GRP78-ACSL4 and GRP78-GPX4 in HSFCs (n = 3), Scale bar: 10 μm. Green color represented ACSL4 or GPX4, red color represented GRP78, and blue color represented DAPI. PCC = Pearson's correlation coefficient. (For interpretation of the references to color in this figure legend, the reader is referred to the Web version of this article.)

4. Discussion

Myopia constitutes the principal cause of visual impairment, and its prevalence has escalated to nearly pandemic proportions. Although scleral ECM remodeling is known to play an important role in myopia progression, which can be induced by hypoxia, ER stress, inflammation and other factors [5–8], effective therapeutic strategies targeting scleral ECM remodeling remain scarce, and advanced therapeutic strategies still need to be developed. Quercetin, as a natural product endowed with rich biological activity, has demonstrated excellent therapeutic potential in diseases related to ER stress and ferroptosis [17–20]. Our previous study had shown that quercetin could alleviate scleral remodeling and control myopia progression [21]. However, given the poor water solubility of quercetin and the challenges posed by ocular physiological barriers when administering therapeutic drugs to posterior ocular tissues, investigating a novel quercetin delivery system to enhance its bioavailability and effectively control myopia progression becomes compelling. In this context, we developed the Exo-Que delivery system to overcome these challenges, and investigated its myopia prevention effects and the therapeutic mechanism in a FDM model. As expected, Exo-Que significantly improve the aqueous solubility of quercetin, enhance permeability and prolong precorneal retention time, which provides sufficient time for drug passage through the cornea, or enter the vascular network such as conjunctival and iris-suprascleral blood vessels. Satisfyingly, the effectiveness of Exo-Que is further strengthened by its enhanced corneal permeability and prolonged retention time, making the effect of myopia prevention comparable to that of atropine, a recognized drug for myopia prevention. After 4 weeks of treatment, Exo-Que could reduce the progression of myopic refractive error by 59.97 %, and inhibited the elongation of AL by 35.85 %, showing a great potential for myopia prevention. Notably, quercetin is naturally distributed in a variety of fruits and vegetables, demonstrating good

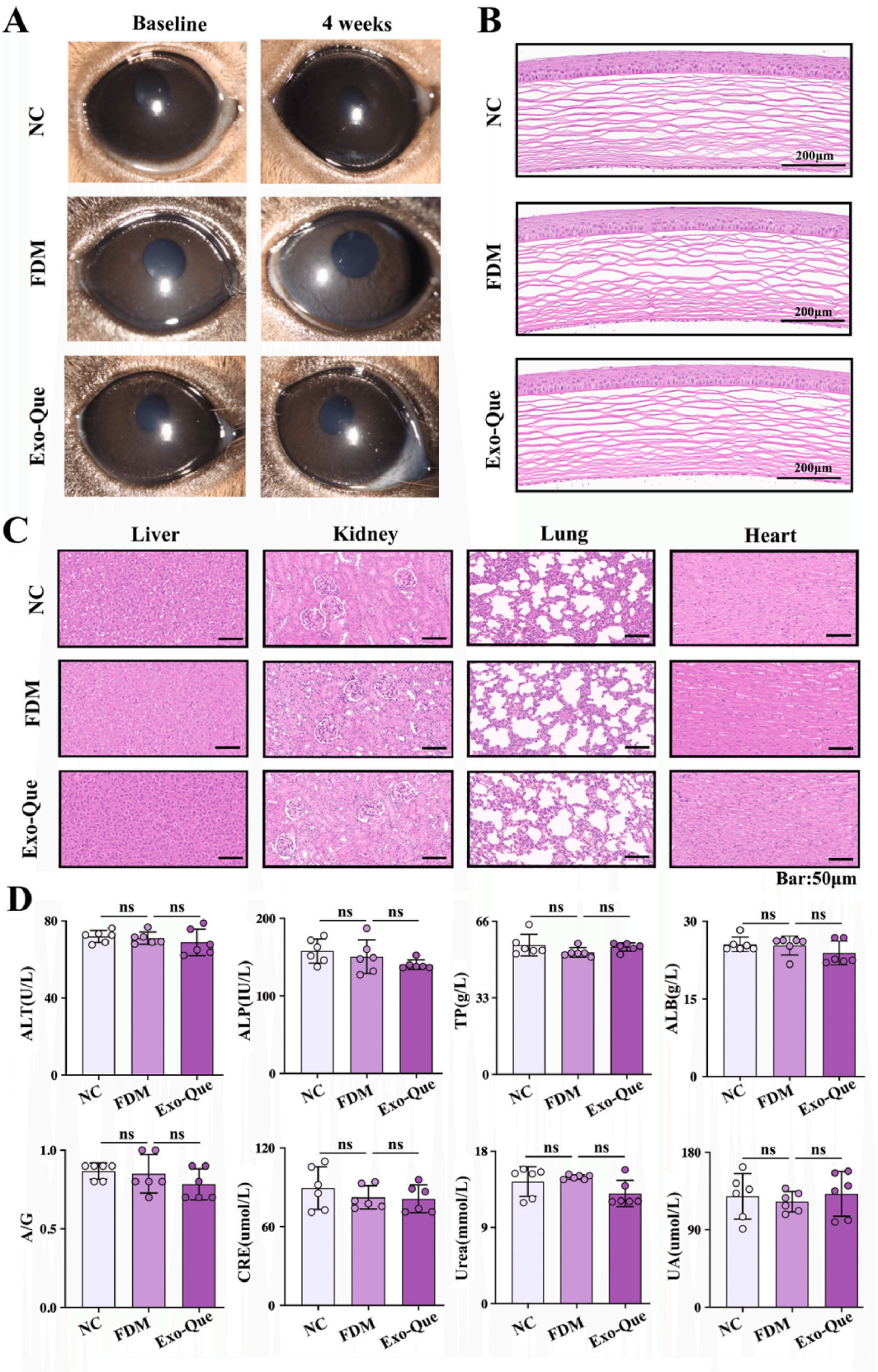

Fig. 10. In vivo biocompatibility assessments of Exo-Que. (A, B) Ocular irritation tests. Slit lamp observation and H&E staining of corneas after PBS and Exo-Que interventions on 4 weeks (n = 3), Scale bar: 200 μm; (C) H&E staining images of main visceral organs, including liver, kidney, lung and heart after different interventions (n = 3), Scale bar: 50 μm; (D) Representative blood biochemistry indices of liver and kidney function (n = 6). ALT, alanine transferase; ALP, alkaline phosphatase; TP, total protein; ALB, albumin; A/G, albumin/globulin; CRE, creatinine; Urea, urea nitrogen; UA, uric acid.

medicinal-food homology. Quercetin can effectively inhibit myopia progression while avoiding safety issues such as mydriasis, photophobia, and allergic reactions associated with high-concentration atropine eye drops. Therefore, it is anticipated to serve as a safe alternative strategy for myopia prevention.

Although Exo-Que has exhibited satisfactory effects, its therapeutic mechanism is not yet fully understood. Exploring the regulation of signaling pathways by Exo-Que during intervention is critical for identifying potential myopia prevention targets. In this study, the scleral fibroblasts of guinea pigs in FDM and FDM + Exo groups showed characteristic morphological alterations of ferroptosis and ER stress. Exo-Que treatment significantly inhibited these morphological changes, confirming that the myopic therapeutic effect of Exo-Que was attributed to quercetin rather than the blank exosomes serving as a vehicle. Given that the activation of ER stress pathways can promote ferroptosis and aggravate tissue damage under some pathological conditions [37–42], and those scleral fibroblasts are responsible for synthesizing all ECM components [3,4], we speculate that ER stress and ferroptosis in scleral fibroblasts involve in scleral ECM remodeling, and that Exo-Que alleviates ECM remodeling by negatively regulating ferroptosis and ER stress. Based on these preliminary findings, we further investigated the parameters associated with ER stress, ferroptosis and scleral ECM remodeling in different groups of scleral tissues. The results confirm that Exo-Que effectively reverse the FD-induced up-regulation of ER stress-related markers GRP78, IRE1, XBP1, PERK, p-eIF2, ATF6, CHOP as well as the ferroptosis-related marker ACSL4, while upregulating the expression of GPX4. Simultaneously, Exo-Que inhibits the accumulation of iron and lipid peroxidation products in the sclera. While Exo-Que inhibit ER stress and ferroptosis, the expression of TGF beta-1 is upregulated and MMP-2 expression fell. These changes could promote collagen accumulation and inhibit its degradation, thereby suppressing scleral ECM remodeling and delaying AL elongation [5,10]. Collectively, all these results demonstrate that Exo-Que could alleviate scleral ECM remodeling by inhibiting ER stress and ferroptosis, presenting a promising strategy for myopia prevention.

Noteworthily, the relationship between ferroptosis and ER stress is highly complex, and the underling mechanisms of their interaction remains elusive. Accumulating evidence indicated that ferroptosis, as a new form of cell death similar to apoptosis and autophagy, is also regulated by ER stress [37,38,43,44]. As reported, ER stress could regulate ferroptosis through PERK-ATF4 pathway [37,43,44], and aggravate ferroptosis-related epithelial-mesenchymal transition progression through XBP1-Hrd1-Nrf2 axis [38]. Xu et al. demonstrated that activation of the AMPK/SIRT1 pathway could inhibit ER stress-mediated ferroptosis through the ATF4-CHAC1 axis [39]. Besides, Guan et al. clarified that exogenous melatonin inhibits hepatic ferroptosis by ameliorating ER stress via the MT2/cAMP/PKA/IRE1 signaling pathway [40]. Consequently, further exploration of the regulatory mechanism between ferroptosis and ER stress is of great significance for elucidating the mechanism of scleral ECM remodeling and screening specific therapeutic targets. In this work, we constructed a protein-protein interaction network of ER stress- and ferroptosis-related proteins, and the results show GRP78 is the key target linking the ER stress and ferroptosis protein interaction networks. Satisfyingly, protein-protein docking and Co-IP assays prove that there were strong protein interactions among GRP78-ACSL4 and GRP78-GPX4. Additionally, immunofluorescence co-localization results confirmed that GRP78-ACSL4 and GRP78-GPX4 were co-localized in the sclera of FDM animals and in the ER stress model of HSCFs. Exo-Que treatment effectively reduced the co-localization of GRP78-ACSL4 while promoting the co-localization of GRP78-GPX4. Given the pivotal roles of GPX4 and ACSL4 in lipid peroxidation and the evidence that overexpression of GRP78 inhibits GPX4 degradation and suppresses ferroptosis [45–50], we speculate that Exo-Que may inhibit the enzymatic activity of ACSL4 by weakening the protein interaction between GRP78 and ACSL4, thereby reducing the accumulation of lipid peroxidation. Concurrently, Exo-Que could enhance the interaction between GRP78 and GPX4, thereby stabilizing the structure of GPX4, preventing its degradation, and ultimately inhibiting lipid peroxidation and alleviating ferroptosis.

Although the therapeutic efficacy of Exo-Que in the FDM model is promising, given safety concerns regarding therapeutic drug administration in adolescents with myopia, verifying its biosafety before clinical application is essential. In this study, we assessed the ocular surface health of guinea pigs using slit-lamp microscopy after continuous administration of Exo-Que for four weeks. Upon examination, it was ascertained that the cornea and conjunctiva appeared healthy, with no signs of inflammation, corneal opacity, or conjunctival hyperemia. Similarly, H&E staining outcomes verified that the corneal epithelial cells were regular and compactly arranged, with no signs of inflammatory infiltration or cytopathology. These results indicate that Exo-Que is well tolerated in the eyes and could be used as a safe mode of ocular administration. In addition, Exo-Que did not show obvious toxic effects in subsequent blood biochemical tests or in morphological studies of important organs, indicating its good biocompatibility and supporting its potential for clinical application.

There are some limitations in the study. The therapeutic efficacy of Exo-Que on myopia was only evaluated in the FDM guinea pig model. Future investigations should extend to other animal models and encompass broader studies to validate these findings. Furthermore, the potential immunogenicity risks associated with human-derived exosomes in guinea pigs, as well as whether physiological differences between guinea pig and human eyes influence drug absorption, necessitate further exploration. The drug-loading efficiency and pharmacokinetic properties of exosomes require optimization to facilitate their translational application in clinical settings. Notably, our study represents the pioneering introduction of an exosome-based drug delivery system for myopia prevention. The developed quercetin-loaded exosome delivery system effectively inhibits myopia progression. Additionally, our research elucidates the previously unexplored role of ferroptosis in myopia, demonstrating that Exo-Que suppresses ferroptosis by modulating the protein interactions of GRP78-ACSL4 and GRP78-GPX4. Collectively, these findings indicate that Exo-Que constitutes a highly promising nanodrug delivery system with transformative potential for myopia treatment, offering a non-invasive and scalable therapeutic strategy applicable in clinical practice.

5. Conclusion

This study successfully established a quercetin-loaded exosome delivery system for myopia treatment. The Exo-Que system improves the solubility, corneal permeability and precorneal retention time of quercetin, thereby enhancing its efficacy. Additionally, Exo-Que alleviates ER stress by inhibiting the IRE1-XBP1, PERK-eIF2 and ATF6 pathways, and may regulate ferroptosis by targeting the GRP78-ACSL4 and GRP78-GPX4 protein interactions to delay myopia progression. Although Exo-Que exhibits favorable efficacy and excellent biocompatibility, further studies are still needed to explore the mechanism of ferroptosis and ER stress in myopia. Optimization of the drug delivery system and evaluation of its safety and effectiveness in preclinical and clinical trials are also required. Overall, our study enhances the understanding of the mechanisms underlying myopia and offers new strategies for its prevention.

CRediT authorship contribution statement

Lianghui Zhao: Writing – original draft, Visualization, Validation, Methodology, Investigation, Conceptualization. **Xiaoyun Dong:** Visualization, Validation. **Bin Guo:** Writing – review & editing, Formal analysis, Data curation, Conceptualization. **Jike Song:** Writing – review & editing, Supervision, Funding acquisition, Formal analysis, Conceptualization. **Hongsheng Bi:** Writing – review & editing, Supervision, Project administration, Funding acquisition, Data curation,

Conceptualization.

Declaration of competing interest

The authors declare that they have no known competing financial interests or personal relationships that could have appeared to influence the work reported in this paper.

Acknowledgments

This work was supported by the Focus on Research and Development Plan in Shandong Province (No. 2021LCZX09), the Natural Science Foundation of Shandong Province (No. ZR2021LZY045), and TCM science and technology project of Shandong Province (No. M−2023075).

Appendix A. Supplementary data

Supplementary data to this article can be found online at https://doi.org/10.1016/j.mtbio.2025.101896.

Data availability

Data will be made available on request.

References

[1] P.N. Baird, S.M. Saw, C. Lanca, J.A. Guggenheim, J.A. Smith Iii, X. Zhou, K. O. Matsui, K.O. Wu, P. Sankaridurg, A. Chia, M. Rosman, E.L. Lamoureux, R. Man, M. He, Myopia, Nat. Rev. Dis. Primers 6 (1) (2020) 99.
[2] M.A. Bullimore, E.R. Ritchey, S. Shah, N. Leveziel, R.R.A. Bourne, D.I. Flitcroft, The risks and benefits of myopia control, Ophthalmology 128 (11) (2021) 1561–1579.
[3] C. Boote, I.A. Sigal, R. Grytz, Y. Hua, T.D. Nguyen, M.J.A. Girard, Scleral structure and biomechanics, Prog. Retin. Eye Res. 74 (2020) 100773.
[4] A.R. Harper, J.A. Summers, The dynamic sclera: extracellular matrix remodeling in normal ocular growth and myopia development, Exp. Eye Res. 133 (2015) 100–111.
[5] H. Wu, W. Chen, F. Zhao, Q. Zhou, P.S. Reinach, L. Deng, L. Ma, S. Luo, N. Srinivasalu, M. Pan, Y. Hu, X. Pei, J. Sun, R. Ren, Y. Xiong, Z. Zhou, S. Zhang, G. Tian, J. Fang, L. Zhang, J. Lang, D. Wu, C. Zeng, J. Qu, X. Zhou, Scleral hypoxia is a target for myopia control, Proc. Natl. Acad. Sci. U.S.A 115 (30) (2018) E7091–E7100.
[6] X. Lin, Y. Lei, M. Pan, C. Hu, B. Xie, W. Wu, J. Su, Y. Li, Y. Tan, X. Wei, Z. Xue, R. Xu, M. Di, H. Deng, S. Liu, X. Yang, J. Qu, W. Chen, X. Zhou, F. Zhao, Augmentation of scleral glycolysis promotes myopia through histone lactylation, Cell Metab. 36 (3) (2024) 511–525.
[7] F. Zhao, H. Wu, P.S. Reinach, Y. Wu, Y. Zhai, Y. Lei, L. Ma, Y. Su, Y. Chen, F. Li, X. Liu, N. Srinivasalu, J. Qu, X. Zhou, Up-regulation of matrix metalloproteinase-2 by scleral monocyte-derived macrophages contributes to myopia development, Am. J. Pathol. 190 (9) (2020) 1888–1908.
[8] D. Hu, J. Jiang, B. Ding, K. Xue, X. Sun, S. Qian, Mechanical strain regulates myofibroblast differentiation of human scleral fibroblasts by YAP, Front. Physiol. 12 (2021) 712509.
[9] S.I. Ikeda, T. Kurihara, X. Jiang, Y. Miwa, D. Lee, N. Serizawa, H. Jeong, K. Mori, Y. Katada, H. Kunimi, N. Ozawa, C. Shoda, M. Ibuki, K. Negishi, H. Torii, K. Tsubota, Scleral PERK and ATF6 as targets of myopic axial elongation of mouse eyes, Nat. Commun. 13 (1) (2022) 5859.
[10] C. Zhu, Q. Chen, Y. Yuan, M. Li, B. Ke, Endoplasmic reticulum stress regulates scleral remodeling in a guinea pig model of form-deprivation myopia, 2020, J. Ophthalmol., 2020 3264525.
[11] P. Walter, D. Ron, The unfolded protein response: from stress pathway to homeostatic regulation, Science 334 (6059) (2011) 1081–1086.
[12] A.V. Cybulsky, Endoplasmic reticulum stress, the unfolded protein response and autophagy in kidney diseases, Nat. Rev. Nephrol. 13 (11) (2017) 681–696.
[13] Z. Zhang, L. Zhang, L. Zhou, Y. Lei, Y. Zhang, C. Huang, Redox signaling and unfolded protein response coordinate cell fate decisions under ER stress, Redox Biol. 25 (2019) 101047.
[14] Z. Pei, Y. Qin, X. Fu, F. Yang, F. Huo, X. Liang, S. Wang, H. Cui, P. Lin, G. Zhou, J. Yan, J. Wu, Z.N. Chen, P. Zhu, Inhibition of ferroptosis and iron accumulation alleviates pulmonary fibrosis in a bleomycin model, Redox Biol. 57 (2022) 102509.
[15] L.F. Luo, P. Guan, L.Y. Qin, J.X. Wang, N. Wang, E.S. Ji, Astragaloside IV inhibits adriamycin-induced cardiac ferroptosis by enhancing Nrf2 signaling, Mol. Cell. Biochem. 476 (7) (2021) 2603–2611.
[16] S.H. Baqer, S.G. Al-Shawi, Z.K. Al-Younis, Quercetin, the potential powerful flavonoid for human and food: a review, Front Biosci (Elite Ed) 16 (3) (2024) 30.
[17] J. Wang, L. Ding, K. Wang, R. Huang, W. Yu, B. Yan, H. Wang, C. Zhang, Z. Yang, Z. Liu, Role of endoplasmic reticulum stress in cadmium-induced hepatocyte apoptosis and the protective effect of quercetin, Ecotoxicol. Environ. Saf. 241 (2022) 113772.
[18] F. Eisvand, A. Tajbakhsh, V. Seidel, M.R. Zirak, J. Tabeshpour, A. Shakeri, Quercetin and its role in modulating endoplasmic reticulum stress: a review, Phytother Res. 36 (1) (2022) 73–84.
[19] L. Ding, S. Dang, M. Sun, D. Zhou, Y. Sun, E. Li, S. Peng, J. Li, G. Li, Quercetin induces ferroptosis in gastric cancer cells by targeting SLC1A5 and regulating the p-Camk2/p-DRP1 and NRF2/GPX4 Axes, Free Radic. Biol. Med. 213 (2024) 150–163.
[20] Y. Wang, F. Quan, Q. Cao, Y. Lin, C. Yue, R. Bi, X. Cui, H. Yang, Y. Yang, L. Birnbaumer, X. Li, X. Gao, Quercetin alleviates acute kidney injury by inhibiting ferroptosis, J. Adv. Res. 28 (2020) 231–243.
[21] M. Zhang, R. Zhang, J. Hao, X. Zhao, Z. Ma, Y. Peng, B. Bao, J. Xin, X. Yin, H. Bi, D. Guo, Quercetin alleviates scleral remodeling through inhibiting the PERK-EIF2α Axis in experiment myopia, Invest. Ophthalmol. Vis. Sci. 65 (13) (2024) 11.
[22] S.N. Hassan, F. Ahmad, Considering dimethyl sulfoxide solvent toxicity to mammalian cells and its biological effects, Exp. Oncol. 46 (2) (2024) 174–178.
[23] Y. Tian, T. Zhang, J. Li, Y. Tao, Advances in development of exosomes for ophthalmic therapeutics, Adv. Drug Deliv. Rev. 199 (2023) 114899.
[24] M. Xu, Q. Yang, X. Sun, Y. Wang, Recent advancements in the loading and modification of therapeutic exosomes, Front. Bioeng. Biotechnol. 8 (2020) 586130.
[25] Q. Tang, B. Lu, J. He, X. Chen, Q. Fu, H. Han, C. Luo, H. Yin, Z. Qin, D. Lyu, L. Zhang, M. Zhou, K. Yao, Exosomes-loaded thermosensitive hydrogels for corneal epithelium and stroma regeneration, Biomaterials 280 (2022) 121320.
[26] Y. Tian, Y. Zhang, J. Zhao, F. Luan, Y. Wang, F. Lai, D. Ouyang, Y. Tao, Combining MSC exosomes and cerium oxide nanocrystals for enhanced dry eye syndrome therapy, Pharmaceutics 15 (9) (2023) 2301.
[27] F. Ma, J. Feng, X. Liu, Y. Tian, W.J. Wang, F.X. Luan, Y.J. Wang, W.Q. Yang, J. Y. Bai, Y.Q. Zhang, Y. Tao, A synergistic therapeutic nano-eyedrop for dry eye disease based on ascorbic acid-coupled exosomes, Nanoscale 15 (4) (2023) 1890–1899.
[28] H. Bao, Y. Tian, H. Wang, T. Ye, S. Wang, J. Zhao, Y. Qiu, J. Li, C. Pan, G. Ma, W. Wei, Y. Tao, Exosome-loaded degradable polymeric microcapsules for the treatment of vitreoretinal diseases, Nat. Biomed. Eng. 8 (11) (2024) 1436–1452.
[29] S.J. Wassmer, L.S. Carvalho, B. György, L.H. Vandenberghe, C.A. Maguire, Exosome-associated AAV2 vector mediates robust gene delivery into the murine retina upon intravitreal injection, Sci. Rep. 7 (2017) 45329.
[30] X. Dong, Y. Lei, Z. Yu, T. Wang, Y. Liu, G. Han, X. Zhang, Y. Li, Y. Song, H. Xu, M. Du, H. Yin, X. Wang, H. Yan, Exosome-mediated delivery of an anti-angiogenic peptide inhibits pathological retinal angiogenesis, Theranostics 11 (11) (2021) 5107–5126.
[31] Y. Tian, F. Zhang, Y. Qiu, S. Wang, F. Li, J. Zhao, C. Pan, Y. Tao, D. Yu, W. Wei, Reduction of choroidal neovascularization via cleavable VEGF antibodies conjugated to exosomes derived from regulatory T cells, Nat. Biomed. Eng. 5 (9) (2021) 968–982.
[32] D. Pollalis, D. Kim, G.K.G. Nair, C. Kang, A.V. Nanda, S.Y. Lee, Intraocular RGD-engineered exosomes and active targeting of choroidal neovascularization (CNV), Cells 11 (16) (2022) 2573.
[33] Y. Chen, Q. Zhu, L. Cheng, Y. Wang, M. Li, Q. Yang, L. Hu, D. Lou, J. Li, X. Dong, L. P. Lee, F. Liu, Exosome detection via the ultrafast-isolation system: EXODUS, Nat. Methods 18 (2) (2021) 212–218.
[34] Q.L. Wang, X. Zhuang, M.K. Sriwastva, J. Mu, Y. Teng, Z. Deng, L. Zhang, K. Sundaram, A. Kumar, D. Miller, J. Yan, H.G. Zhang, Blood exosomes regulate the tissue distribution of grapefruit-derived nanovector via CD36 and IGFR1 pathways, Theranostics 8 (18) (2018) 4912–4924.
[35] Y. Cui, Y. Guo, L. Kong, J. Shi, P. Liu, R. Li, Y. Geng, W. Gao, Z. Zhang, D. Fu, A bone-targeted engineered exosome platform delivering siRNA to treat osteoporosis, Bioact. Mater. 10 (2021) 207–221.
[36] J. Feng, X. Chen, R. Li, Y. Xie, X. Zhang, X. Guo, L. Zhao, Z. Xu, Y. Song, J. Song, H. Bi, Lactylome analysis reveals potential target modified proteins in the retina of form-deprivation myopia, iScience 27 (9) (2024) 110606.
[37] T. Zeng, Y. Zhou, Y. Yu, J.W. Wang, Y. Wu, X. Wang, L. Zhu, L.M. Zhou, L.H. Wan, rmMANF prevents sepsis-associated lung injury via inhibiting endoplasmic reticulum stress-induced ferroptosis in mice, Int. Immunopharmacol. 114 (2023) 109608.
[38] Z. Liu, P. Nan, Y. Gong, L. Tian, Y. Zheng, Z. Wu, Endoplasmic reticulum stress-triggered ferroptosis via the XBP1-Hrd1-Nrf2 pathway induces EMT progression in diabetic nephropathy, Biomed. Pharmacother. 164 (2023) 114897.
[39] J. Xu, L. Zhao, X. Zhang, K. Ying, R. Zhou, W. Cai, X. Wu, H. Jiang, Q. Xu, D. Miao, Y. Zeng, F. Yu, Salidroside ameliorates acetaminophen-induced acute liver injury through the inhibition of endoplasmic reticulum stress-mediated ferroptosis by activating the AMPK/SIRT1 pathway, Ecotoxicol. Environ. Saf. 262 (2023) 115331.
[40] Q. Guan, Z. Wang, K. Hu, J. Cao, Y. Dong, Y. Chen, Melatonin ameliorates hepatic ferroptosis in NAFLD by inhibiting ER stress via the MT2/cAMP/PKA/IRE1 signaling pathway, Int. J. Biol. Sci. 19 (12) (2023) 3937–3950.
[41] M.D. Li, L. Fu, B.B. Lv, Y. Xiang, H.X. Xiang, D.X. Xu, H. Zhao, Arsenic induces ferroptosis and acute lung injury through mtROS-mediated mitochondria-associated endoplasmic reticulum membrane dysfunction, Ecotoxicol. Environ. Saf. 238 (2022) 113595.
[42] S. Wang, F. Xu, H. Liu, Y. Shen, J. Zhang, L. Hu, L. Zhu, Suppressing endoplasmic reticulum stress alleviates LPS-induced acute lung injury via inhibiting inflammation and ferroptosis, Inflammation 47 (4) (2024) 1067–1082.
[43] C. Zhao, D. Yu, Z. He, L. Bao, L. Feng, L. Chen, Z. Liu, X. Hu, N. Zhang, T. Wang, Y. Fu, Endoplasmic reticulum stress-mediated autophagy activation is involved in cadmium-induced ferroptosis of renal tubular epithelial cells, Free Radic. Biol. Med. 175 (2021) 236–248.

[44] Y. Chen, Y. Mi, X. Zhang, Q. Ma, Y. Song, L. Zhang, D. Wang, J. Xing, B. Hou, H. Li, H. Jin, W. Du, Z. Zou, Dihydroartemisinin-induced unfolded protein response feedback attenuates ferroptosis via PERK/ATF4/HSPA5 pathway in glioma cells, J. Exp. Clin. Cancer Res. 38 (1) (2019) 402.
[45] I. Ingold, C. Berndt, S. Schmitt, S. Doll, G. Poschmann, K. Buday, A. Roveri, X. Peng, F. Porto Freitas, T. Seibt, L. Mehr, M. Aichler, A. Walch, D. Lamp, M. Jastroch, S. Miyamoto, W. Wurst, F. Ursini, E.S.J. Arnér, N. Fradejas-Villar, U. Schweizer, H. Zischka, J.P. Friedmann Angeli, M. Conrad, Selenium utilization by GPX4 is required to prevent hydroperoxide-induced ferroptosis, Cell 172 (3) (2018) 409–422.
[46] W.S. Yang, R. SriRamaratnam, M.E. Welsch, K. Shimada, R. Skouta, V. S. Viswanathan, J.H. Cheah, P.A. Clemons, A.F. Shamji, C.B. Clish, L.M. Brown, A. W. Girotti, V.W. Cornish, S.L. Schreiber, B.R. Stockwell, Regulation of ferroptotic cancer cell death by GPX4, Cell 156 (1–2) (2014) 317–331.
[47] P. Liao, W. Wang, W. Wang, I. Kryczek, X. Li, Y. Bian, A. Sell, S. Wei, S. Grove, J. K. Johnson, P.D. Kennedy, M. Gijón, Y.M. Shah, W. Zou, CD8+T cells and fatty acids orchestrate tumor ferroptosis and immunity via ACSL4, Cancer Cell 40 (4) (2022) 365–378.
[48] Q.Z. Tuo, Y. Liu, Z. Xiang, H.F. Yan, T. Zou, Y. Shu, X.L. Ding, J.J. Zou, S. Xu, F. Tang, Y.Q. Gong, X.L. Li, Y.J. Guo, Z.Y. Zheng, A.P. Deng, Z.Z. Yang, W.J. Li, S. T. Zhang, S. Ayton, A.I. Bush, H. Xu, L. Dai, B. Dong, P. Lei, Thrombin induces ACSL4-dependent ferroptosis during cerebral ischemia/reperfusion, Signal Transduct. Targeted Ther. 7 (1) (2022) 59.
[49] J. Cui, Y. Chen, Q. Yang, P. Zhao, M. Yang, X. Wang, G. Mang, X. Yan, D. Wang, Z. Tong, P. Wang, Y. Kong, N. Wang, D. Wang, N. Dong, M. Liu, M. E, M. Zhang, B. Yu, Protosappanin a protects DOX-induced myocardial injury and cardiac dysfunction by targeting ACSL4/FTH1 axis-dependent ferroptosis, Adv. Sci. 11 (34) (2024) e2310227.
[50] S. Zhu, Q. Zhang, X. Sun, H.J. Zeh 3rd, M.T. Lotze, R. Kang, D. Tang, HSPA5 regulates ferroptotic cell death in cancer cells, Cancer Res. 77 (8) (2017) 2064–2077.